https://doi.org/10.5194/cp-2020-35
Preprint. Discussion started: 13 May 2020

Climate of the Past
Discussions

Early Jurassic climate and atmospheric CO_2 concentration in the Sichuan paleobasin, Southwest China

Xianghui Li[1], Jingyu Wang[1], Troy Rasbury[2], Min Zhou[1], Zhen Wei[1], Chaokai Zhang[1]

[1]State Key Laboratory for Mineral Deposits Research, School of Earth Sciences and Engineering, Nanjing University, Nanjing 210023 China.

[2]Department of Geosciences, Stony Brook University, Stony Brook, NY 11794-2100, USA

Correpondence to: Xiangui Li (leeschhui@126.com)

https://doi.org/10.5194/cp-2020-35
Preprint. Discussion started: 13 May 2020

Climate of the Past Discussions
Open Access

Abstract:

Unlike marine archives, terrestrial sediments show more complicated and dynamic environment and climate. This work presents new results of climate-sensitive sediment observation and carbon-oxygen isotope analyses of lacustrine and pedogenic carbonates for the Early Jurassic Ziliujing Formation from the grand Sichuan paleobasin (GSB), Southwest China. Lithofacies analysis indicates calcisols were widespread in riverine and flood plain facies. Climate–sensitive sediments and carbon-oxygen isotopes with palynofloral assemblages manifest that an overall (semi-) arid climate dominated the GSB; and that it became drier through time, accompanied by occasional evaporites in the Toarcian. This climate pattern is similar with the arid climate in Colorado Plateau, western America, but distinct from the relatively warm-humid climate in North China and northern Gondwanaland in Southern Hemisphere. The estimated Early Jurassic atmospheric CO_2 concentration (pCO_2) from carbon isotopes of pedogenic carbonates shows a range of 980-2610 ppmV (~ 3.5-10 times the pre-industrial value) with a mean 1660 ppmV. Three phases of pCO_2 (the Sinemurian 1500-2000 ppmV, the Pliensbachian 1000-1500 ppmV, and the early Toarcian 1094-2610 ppmV) and two events of rapid falling pCO_2 by ~1000-1300 ppmV are observed, illustrating the pCO_2 perturbation in the Early Jurassic. The pattern and associated rapid falling events of pCO_2 are compatible with the excursions of stable isotopes and seawater temperature from the coeval marine sediments, consistent with a positive feedback of climate to pCO_2 through the Early Jurassic.

https://doi.org/10.5194/cp-2020-35
Preprint. Discussion started: 13 May 2020

1. Introduction

The Jurassic was a typical greenhouse period with global paleotemperatures possibly 5-10 °C higher than present based on modelling results (e.g., Chandler et al., 1992; Rees et al., 1999; Sellwood and Valdes, 2008). The Early Jurassic epoch was an interval of extreme environmental change, during which climate events were recorded by highly enhanced organic carbon burial, multiple isotopic anomalies, clay mineral composition, oceanic anoxic regime, global sea-level change, vegetation turnover, and mass extinction (e.g. Price, 1999; Hesselbo et al., 2000; Dera et al., 2009; Jenkyns, 2010; Korte and Hesselbo, 2011; Riding et al., 2013; Arabas et al., 2017) as well as $p\mathrm{CO_2}$ perturbation (e.g., Beerling and Royer, 2002; McElwain et al., 2005; Berner, 2006; Retallack, 2001a, 2009; Steinthorsdottir and Vajda, 2015). Recently, examples of rapid transitions from cold, or even glacial, climates to super greenhouse events are documented in some intervals of the Jurassic (e.g., van de Schootbrugge et al., 2005; Suan et al., 2010; Gómez et al., 2016; Arabas et al., 2017). The study of these deep-time climate events may serve as analogues for present-day and future environmental transitions (Hesselbo et al., 2013).

Though the climate events in the Early Jurassic epoch are largely based on the marine sedimentary and geochemical records, data from the terrestrial realm provide important details of environmental change (e.g., Hesselbo et al., 2000; Suan et al., 2010; Jenkyns, 2010; Philippe et al., 2017). Terrestrial proxies, such as flora (e.g., Riding et al., 2013; Deng et al., 2017; Philippe et al., 2017; Ros-Franch et al., 2019), vegetation (Pole, 2009), and geochemistry (e.g., Riding et al., 2013; Kenny, 2015; Tramoy et al., 2016) have begun to provide important information of the Mesozoic-Cenzoic climate and environmental changes on continents. Particularly, a negative feedback in the global exogenic carbon cycle, from carbon isotopes of lacustrine organic matter, has been hypothesized to account for the Toarcian oceanic anoxic event (Xu et al., 2017), opening a new avenue to link marine and terrestrial climate in the Early Jurassic. However, few relatively continuous terrestrial climate records and coupled environmental changes have been documented for the Early Jurassic.

There are several large Triassic-Jurassic terrestrial basins in West China, providing a great opportunity to recover the coeval terrestrial environment and climate. The Sichuan Basin has a relatively complete and continuous sedimentary sequence of the Upper Triassic-Paleogene (e.g., SBGM, 1991, 1997; Wang et al., 2010). Correspondingly, the sedimentary archive could play a key role in the global Early Jurassic correlation of the marine and terrestrial climate. In this work, we present new results of field investigation, lithofacies and paleosol recognition, carbon-oxygen isotope analyses of both lacustrine and pedogenic carbonates, and $p\mathrm{CO_2}$ estimates in the Early Juassic terrestrial Sichuan paleobasin, and we discuss the relationship of terrestrial climatic change to that of the marine counterpart.

2. Geological setting and stratigraphy

Southwest China, including the provinces of Yunnan, Sichuan, Chongqing, and Guizhou, had been the main part of the upper Yangtze Plate since the Proterozoic, possibly since the Neoarchean. With the amalgamation of the Cathaysia and

https://doi.org/10.5194/cp-2020-35
Preprint. Discussion started: 13 May 2020

Yangtze plates, it became the western South China plate or cratonic basin in the Neoproterozoic (Sinian), and marine Neoproterozoic through the Middle Triassic strata is well preserved. With the Indosinian orogeny, new foreland basins were formed since the Late Triassic (e.g., He and Liao, 1985; Li et al., 2003), which record the Mesozoic and Cenozoic evolution of tectonics, environment, and climate in Southwest China.

The Mesozoic Sichuan paleobasin was confined by the Longmenshan thrust belt in the northwest, the Micangshan-Dabashan arcuate thrust belt in the northeast (Fig. 1), and the northern hilly topography boundary of the Yunnan-Guizhou plateau in the south and east. It was mainly developed during the Late Triassic-Jurassic and includes provincial areas of eastern Sichuan, entire Chongqing, northern Guizhou, western Hubei, and northwestern Hunan. This Triassic-Jurassic Sichuan foreland basin was much larger than the present Sichuan Basin in the eastern Sichuan province. We estimate the size of Sichuan paleobasin is roughly 480,000 km^2 by the lithofacies paleogeography (Fig. 1. Ma et al., 2009; Li and He, 2014), and suggest naming this the grand Sichuan paleobasin (GSB).

The Mesozoic terrestrial sediments accumulated up to ~9 km (Guo et al., 1996) in the GSB; and the Jurassic part can be as much as 3-3.5 km thick (SBGM, 1991). Two types of Lower Jurassic deposits have been distinguished (Table 1): the Baitianba Formation (Fm) in the north and the Ziliujing Fm (e.g., SBGM, 1991; Wang et al., 2010) in the south (over 90% of the basin).

The Baitianba Fm was deposited unconformably on the Upper Triassic Xujiahe Fm and is overlain conformably by the Middle Jurassic Xintiangou Fm / Qianfuyan Fm (Table 1). It is mainly composed of grayish shales and sandstones with coal layers and massive conglomerates. Abundant plant fossils, sporopollens, conchostracans, bivalves, and gastropods indicate it is the Early Jurassic (SBGM, 1991, 1997). Sporopollen assemblages of the Hettangian-Sinemurian age were found in the lower part (Zhang and Meng, 1987) and the Pliensbachian-Toarcian assemblages were reported in the upper part (Wang et al., 2010).

The Ziliujing Fm is composed of variegated and reddish mudrocks (some shales) intercalated with sandstones, siltstones, and bioclastic limestones as well as marlstones, conformably or unconformably overlying the Xujiahe Fm or Luqiao Fm and conformably underlying the Xintiangou Fm (SBGM, 1997. Table 1). It has been dated as the Early Jurassic by fossil assemblages of dinosaurs, bivalves, ostracods, conchostracans, and plants, within which the dinosaur fauna can be well correlated to the Lufeng Fauna in central Yunnan (e.g., Dong, 1984; SBGM, 1991, 1997; Peng, 2009). This formation is subdivided as five parts in an ascending order: the Qijiang, Zhenzhuchong, Dongyuemiao, Ma'anshan, and Da'anzhai members (SBGM, 1997. Table 1). Of them, the former two are sometimes combined the Zhenzhuchong Fm (e.g., SBGM, 1991; Wang et al., 2010).

The Da'anzhai Member is characterized by dark gray to black shales and bioclastic limestones with a southward increase of reddish mudrocks (SBGM, 1991, 1997; Wang et al., 2010), which has been mainly regarded the sediment in a grand Sichuan paleolake (e.g., Ma et al., 2009; Li and He, 2014). Ostracod assemblagse indicate it is the late Early Jurassic (e.g., Wei, 1982;

https://doi.org/10.5194/cp-2020-35
Preprint. Discussion started: 13 May 2020

Wang et al., 2010). A Re–Os isochron age 180.3 ± 3.2 Ma combined with the organic carbon isotope excursion indicates that the lower Da'anzhai Member corresponds to the Toarcian Oceanic Anoxic event (T-OAE. Xu et al., 2017), consistent with the assigned Toarcian age.

The Ma'anshan Member is comprised of violet-red mudrocks with a few greyish, greenish thin-bedded fine sandstones and siltstones, in which floral fossils are common (Li and Meng, 2003). The Dongyuemiao Member consists of greenish and reddish mudrocks and siltstones with greyish bioclastic limestone and marlstone, of which abundant bivalve and plant fossils were reported from eastern Sichuan and Chongqing (Li and Meng, 2003; Meng et al., 2003; Wang et al., 2010). The Zhenzhuchong Member is dominated by violet red mudrocks/shales intercalated with thinned sandstones and / or siltstones and numerous plant fossils of the Early Jurassic affinity (e.g., Duan and Chen, 1982; Ye et al., 1986). Taken together, fossil associations suggest that the three members were deposited in the middle-late Early Jurassic. The age limitation of the overlying Da'anzhai Member and the correlation to the Lufeng dinosaur fauna places these members in the Sinemurian – Pliensbachian, and the Zhengzhuchong and Dongyuemiao Fms are temporally suggested the Sinemurian age (Table 1).

The Qijiang Member is composed of quartz arenite interbedded/intercalated with dark shales. Coal seams can be often seen in the middle of the Qijiang Member. This member mainly occurs in the central part of the GSB. It is likely the earliest Jurassic, possibly Hettangian age, but plant fossils cannot precisely indicate the age (Wang et al., 2010).

3. Materials and methods

Observation and description for sedimentary facies analysis were executed on six outcrop sections (Locations A1 to A4, A6 and A7, Fig. 1). Published description for other sections (Locations A5, A8, and A9, Fig. 1) is integrated into our observations. Details of microscopic examination of sedimentary rocks and sedimentary facies analysis which are the underpinning of climate analsysis are attached as the supplementary data Note S1. Below are chiefly introduced materials and methods of climate-sensitive sediment observation, carbon-oxygen isotope analyses, and estimate of $p\mathrm{CO_2}$.

3.1. Observation of climate-sensitive sediments

Climate-sensitive sediments are mainly the dolomites, gupsum, and paleosols, which are used to analyze the climate in this work.

Dolomites and gupsum are relatively easy to recognize in both field and under microscope. We distinguish dolomites from limetstones following Tucker (2003) and Flügel (2004). As Flügel (2004) stated, field distinctions of limestone and dolomite can also be made although detailed differentiation of carbonate rocks is best performed in the laboratory. The basic method that we use to examine dolomites is: limestone will fizz strongly and dolomite will show little or no reaction when add dilute 10 % hydrochloric acid on carbonate (Flügel, 2004); and limestone will stain pink to mauve but dolomite will be unstained

https://doi.org/10.5194/cp-2020-35
Preprint. Discussion started: 13 May 2020

(e.g., Tucker, 2003; Flügel, 2004) when Alizarin-red S in weak HCl is added on freash outcrop or coverslip-free thin section. Gypsum is recognizable by properties of low Mohs hardness (2) and transparence to translucence. In field, we also recognize gypsum by particular structures such as chichen-wire cage, gypsum pseudomorph, and cluster of (0.5-1 cm) pore.

There are multiple classifications of paleosols (e.g., Wright, 1992; Mack et al., 1993; Retallack, 2001b; Imbellone, 2011), mostly based on the US Soil Taxonomy. We recognized paleosols in the field based on color, structures, horizonation, root traces, and textures, and followed the general classification paleosols by Mack et al. (1993) and Retallack (2001b). In this paper, paleosols were described following the procedures of the Soil Survey Manual and classified according to Soil Survey Staff (1998).

Within the measured and observed sections, paleosol profiles were mainly identified from the two main locations/sections A4 and A6 (Figs. S1 and S2, and Table S1). Horizonation, BK horizon thickness, boundary condition, structures, trace fossils, rootlets, carbonate accumulations (calcretes), etc. were observed and described (Table S1). Paleosols interpreted in other cited sections (Fig. 1) rely on the diescription of lithology, strcucture, and calcrete in the original references.

Based upon a modification of the Retallack (1998) categorization of paleosol maturity, the relative paleosol development (maturity) was assigned.

3.2. Analyses of carbon-oxygen isotopes

Ten lacustrine carbonate samples were collected to analyse carbon-oxygen isotopes from the Da'anzhai Member of the Ziliujing Fm at the Shaping section, Ya'an (Location A4. Fig. S1 and Table S3). Twenty-six pedogenic carbonate samples were selected to measure carbon-oxygen isotopes from thirty-one paleosol horizons of the Ziliujing Fm at the same section (Fig. S1 and Table S4). Two or three microdrilling powder samples (columns 7 and 8 in Table S4) were taken from the same individual calcrete for stable isotope analysis, and then a mean value for each calcrete sample was calculated (columns 9 and 10 in Table S4).

Before drilling, diagenetic fabrics of samples were studied under a microscope. Each sample was cut and prepared as thin sections for diagenetic diagnosis, and cathodoluminescence (CL) images (Fig. 2) were used to examine if the calcites were evenly precipitated. Only the areas that were a uniform (often orange) luminescene (Fig. 2) were microsampled for isotope analyses. Cracks, veins, and vug spaces in concretion samples were found to be filled by multidirectional growth of spar crystals. These crack spar fills were avoided when microsampling as they were interpreted as recrystallization and replacement diagenetic phases. Microsampling of lacustrine carbonate samples focused on avoiding spar and sampling only micrites. Powder samples were obtained by dentist drilling machine (aiguille diameter ϕ=1-2 mm).

Isotopic analyses were conducted on 0.3 ~ 0.5 mg powder samples. Powder samples were dried in an oven at 60˚C for 10 hours before being moved to the instrument. Carbon dioxide for isotopic analysis was released using orthophosphoric acid at 70˚C and analysed on-line in a DELTA-Plus xp (CF-IRMS) mass spectrometer at the State Key Laboratory for Mineral

https://doi.org/10.5194/cp-2020-35
Preprint. Discussion started: 13 May 2020

Deposits Research, Nanjing University. The precision of the measurements was regularly checked with a Chinese national carbonate standard (GBW04405) and the international standard (NBS19) and the standard deviation of $\delta^{13}C$ was ±0.1‰ over the period of analysis. Calibration to the international PeeDee Belemnite (PDB) scale was performed using NBS19 and NBS18 standards.

3.3. Calculation of atmospheric CO_2 concentration

There are multiple methods to reconstruct the concentration of atmospheric carbon dioxide, i.e., pCO_2, in deep time. It can be determined from the $\delta^{13}C$ value of pedogenic carbonate using a paleobarometer model (Cerling, 1999), and the reconstruction of pCO_2 has been applied in the climate study of the Mesozoic time (e.g., Ekart et al., 1999; Nordt et al., 2003; Myers et al., 2012; Li et al., 2014; Zhang et al., 2018).

The Cerling (1999) equation was used to calculate the pCO_2 using the carbon isotope of pedogenic carbonates as below:

$$C_a = S_{(z)}(\delta^{13}C_s - 1.0044\delta^{13}C_r - 4.4)/(\delta^{13}C_a - \delta^{13}C_s)$$

where C_a is pCO_2; $\delta^{13}C_s$, $\delta^{13}C_r$, $\delta^{13}C_a$ are the isotopic compositions (‰) of soil CO_2, soil-respired CO_2, and atmospheric CO_2, respectively; and $S_{(z)}$ is the CO_2 contributed by soil respiration (ppmV). Details of parameter usage and selection for the pCO_2 calculation are in the supplememtary data Note S2.

4. Results

Based on the investigation of cross-sections (locations A1-A4, and A6-A7. Fig. 1), we have classified six sedimentary facies units in the Ziliujing Fm. They are alluvial fan, fluvial river, flood plain, lake, lake-delta, and swamp facies. Details of description and interpretation are in the supplementary data Note S1. Below are results of climate-sensitive sediment observation, stable isotope analyses, and pCO_2 calculation.

4.1. Climate-sensitive sediments

Field observation combined with published calcrete materials shows that paleosols widely occur in the Lower Jurassic Ziliujing Fm of the GSB (Figs. 1, 3, and 4). A total of 32 paleosols were observed and described at the Shaping section, Ya'an, and five paleosols were found at the Tanba section, Hechuan (Table S1).

Most of paleosols are reddish (GSA Munsell Rock-Color 5R 2/2, 5R 3/4, 5R 4/2) and brownish (10R 3/4, 10R 5/4) (Fig. 3 and Table S1). Peds of paleosols are mainly angular and subangular, and a few are prismatic and platy. Slickensides are common. Mottles (Fig. 3a), rootlets /rhizoliths (Fig. 3c), and burrows sometimes occur with strong leaching structures (Fig. 3a). Occasionally mudcracks are associated with the aforementioned structures (Fig. 3d).

All paleosols are calcic with more or less calcretes in Bk horizons. The thickness of Bk horizons is mainly 30-50 cm and 50-100 cm, and partly 100-170 cm (Table S1). Calcretes are generally ginger-like, ellipsoid, subglobular, and irregular in shape (Fig. 3b and 3e) and nodules are 1-3 cm even up to 8-15 cm (paleosols J1z-10-01 and J1z-12-01) in size (Fig. 3e). Calcrete is often less than 0.5-1% in an individual paleosol horizon, but a few can be up to 3-5% (paleosol J1z-3-01. Fig. 3b) even 10% (paleosols J1z-5-02 and 18HC-10).

Based on the description of the paleosols described above, all are defined as relatively mature calcisols (Mack et al., 1993), a kind of aridisol (Soil Survey Staff, 1998; Retallack, 2001b). The original lithofacies were chiefly argillaceous and silty (split-fan) overbank, interchannel, and flood plain deposits (Figs. S1 and S2). Some formed landshare of the paleo-lakeshore.

Dolomites were found at seven loactions in central and southern GSB (Figs. 1, 4, and Table S2), which are to some degree an indicative of arid/evapoatre climate. The dolomites chiefly occur in the Toracian Da'anzhai Member and a few in the Sinemurian-Plienbachian Dongyuemiao and Ma'anshan members (Fig. 4). They are often massive whitish (Figs. 3f and S3e) and micritic (Figs. S4b and S4d), likely indicating a syndepositional origin.

Gypsum is only recorded in two loactions (Figs. 1, 4, and Table S2). One is located at Zigong (Location A5. SBG, 1980a). The other lies at Hechuan (Location A6), which can be idientifed by chicken-wire cage structure and is associated with micriditic dolomites (Fig. 3f).

4.2. Carbon-oxygen isotope values

$\delta^{13}C$ values of lacustrine carbonate samples range from -2.02‰ to -4.07‰ and $\delta^{18}O$ values range from -9.91‰ to -12.28‰ (Table S3 and Fig. 5). A distinct increasing trend of both carbon and oxygen isotope ratios can be detected from lower to upper horizons across a 40 m stratal interval of the lower Da'anzhai Member (Fig. 6).

Pedogenic carbonate samples have $\delta^{13}C$ values from -3.52‰ to -8.10‰, which fall in the tyical stable isotope range for pedogenic carbonates. Values of -6‰ to -8.0‰ characterize the sequence of the Zhenzhuchong Member and main Ma'anshan Member, with an abrupt increase to -5.5‰ to -3.5‰ at the top of Ma'anshan Member (samples J1z-16-01 and J1z-18-01. Fig. 6). $\delta^{18}O$ values are mainly from -11.3‰ to -13.10‰ in the interval of the Zhenzhuchong Member and Ma'anshan Member. $\delta^{18}O$ follows $\delta^{13}C$ with a sudden increase to -5.5‰ at the top of the Ma'anshan Member (Fig. 6). Large and frequent variations of both carbon and oxygen isotope ratios can be observed in the lower Da'anzhai Member (Fig. 6 and Table S4).

4.3. CO_2 concentrations

pCO_2 values of the Early Jurassic paleosols vary when different parameters are selected for calculation.

If $S_{(z)}$=2500 ppmV and $\delta^{13}C_a$=-6.5‰ (constant preindustrial atmosphere), pCO_2 values range between ~1140 ppmV and ~3460 ppmV with a mean of 1870 ppmV (column 15 in Table S4); and when $S_{(z)}$=2500 ppmV and $\delta^{13}C_a=(\delta^{13}C_r+18.67)/1.1$, pCO_2 values change between ~1230 ppmV and ~3260 ppmV with a mean of 2070 ppmV (column 16 in Table S4).

If $S_{(z)}$=2000 ppmV and $\delta^{13}C_s$=-8.98+$\delta^{13}C_c$ are used, pCO_2 values are ~ 940-2530 ppmV with the mean 1600 ppmV (column 17 in Table S4); and if $S_{(z)}$=2000 ppmV and $\delta^{13}C_s = (\delta^{13}C_c+1000) / ((11.98-0.12*25) / 1000+1) -1000$ are adopted, pCO_2 values become ~980 ppmV to ~2610 ppmV with the mean 1660 ppmV (column 18 in Table S4). Details of the different parameters and pCO_2 results can be seen in Table S4.

Results further show that pCO_2 values at $S_{(z)}$=2500 ppmV are larger than at $S_{(z)}$=2000 ppmV, and the discrepancy of the highest pCO_2 is ~ 1000 (3640-2610) ppmV, but that of the lowest value is ~300 (1230-930) ppmV and that of the mean value is ~ 370 (2070-1600) ppmV. In addition, when $S_{(z)}$ is the same, the pCO_2 values are close even if other parameters are different (comp. between columns 15 and 16, 17 and 18 in Table S4, and Fig. 6).

However, the trend of pCO_2 over the epoch is quite similar using different values of $S_{(z)}$ and other parameters (Fig. 6). We chose S(z)=2000 ppmV (column 18 in Table S4) to illustrate the nature of the Early Jurassic pCO_2 estimated from calcisols in the GSB.

pCO_2 values mostly range between 980 ppmV and 2610 ppmV, and the mean 1660 ppmV is ~6 times the 275 ppmV. Most of the pCO_2 values are 1000-2000 ppmV with the mean 1580 ppmV in the Zhenzhuchong and Ma'anshan members, ~3.5-7.5 times the pre-industrial pCO_2 value.

5. Discussion

Results show that the depositional environment and paleoclimate in the Early Jurassic were distinctly different from those in the Late Triassic in Southwest China. As a whole, the climate became dry and pCO_2 varied in three phases through the Early Jurassic.

Sedimentary facies analysis indicates two lithofacies cycles were developed and calcisols were largely spread in the Lower Jurassic Ziliujing Fm in the GSB, Southwest China. The first cycle is the riverine and flood plain lithofacies of the Qijiang Membe and Zhenzhuchong Member succeeded by the lacustrine facies of the Dongyuemiao Member, and the second is the flood plain and river facies with swamp lithofacies of the Ma'anshan Member followed by the lacustrine facies of the Da'anzhai Member. We interpret the two packages to reflect two major lake stages (for details refer to supplementary data Note S1).

With the change of depositional environments, paleoclimate and pCO_2 changed, as reflected by climate-sensitive facies and stable isotope analyses.

5.1. Paleoclimate variation

During the Late Triassic, Southwest China was warm-hot and humid in a tropical and subtropical zone, as demonstrted by palynoflora, coals, and perennial riverine and lacustrine lithofacies in the Xujiahe Fm (e.g., Huang, 1995; Xu et al., 2015; Li et al., 2016; Yang et al., 2019), and a distinct transfer of climate took palce in the Early Jurassic manifested by

https://doi.org/10.5194/cp-2020-35
Preprint. Discussion started: 13 May 2020

climate-senstive sediments and stable isotopes of the Ziliujing Fm in GSB.

1) The Hettangian Age

By the Hettangian time (the Qijiang Member), a warm-humid climate followed the Late Triassic in the GSB. The limited sedimentary records are mainly mature quartz sandstones and siltstones with coals and siderite concretions (Fig. 7), indicating a stable tectonic setting and warm-humid climate in the eastern and southern GSB. In the northern margin, the climate was similar, because multiple coal layers occur in the lower Baitianba Fm and the hosted alluvial fan system (Figs. 7 and S6) is characterized by moderate-good roundness and sorting of gravels with sandy fillings (Fig. S3a. e.g., Liu et al., 2016; Qian et al., 2016; and this work). In the Newark basin of eastern America, climate-sensitive sediments such as nodules of carbonate and gypsum (pseudomorph) as well as mudcrack in mudflat facies indicate an arid climate in the fifth cycle of the Hettangian (>199 Ma. Kent et al., 2017) Passaic Fm (Smoot and Olsen, 1994). More widespread, the eolian Navajo Sandstone, dated as Hettangian-Sinemurian (200-195 Ma. Parrish et al., 2019), indicate an arid climate in Colorado Plateau. Obvieously, the arid climate in western America was different from that in the GSB at the time.

2) The Sinemurian Age

The early Sinemurian Zhenzhuchong Member is of riverine and flood plain facies with lacustrine facies, in which the lithology is dominated by violet-red mudrocks with few thin greyish, greenish fine sandstones and siltstones. The reddish color of rocks may indicate a change of climate even if there is little difference in the appearance of reddish color sediment in the western and central basin. That is, the reddish rocks developed through the whole member in the western margin (Location A4. Fig. 6), but it started in the middle member in the central basin (Location A6. Fig. S2).

With the red color mudrocks, a kind of climate-sensitive pedogenesis is recognized from the flood plain facies. Multiple calcisol horizons were observed at the Shaping section, Ya'an (Location A4. Figs. 1, 4, and 7), within which a strong leaching calcisol horizon can be found (Fig. S3c). Calcisols were also interpreted with the description of abundant calcretes at sections of Dafang (Location A8. Zhang et al., 2016), Tianzhu (Location A9. Li and Chen, 2010), and Weiyuan (Location A10. SBG, 1980a), respectively. Calcisols indicate that a (semi-) arid climate at least began to replace the previous humid climate in western and southern margins of the basin (Figs.1, 4, and 7 and Table S2). This climate change, indicated from paleosols, is consistent with the climatic signal from floral fossils (e.g., Huang, 2001; Wang et al., 2010), suggesting a decrease in humidity and an increase in temperature across the interval, compared to that in the Hettangian Qijiang Member and Late Triassic Xujiahe Fm. However, the climate was not distinct in humidity and temperatue in the northern GSB without proxies of sediments and flora even though alluvial fan and lacustrine delta facies are common in the middle of the Baitianba Fm (Fig. S6. e.g., Qian et al., 2016).

No climate-sensitive sediments are documented in the late Sinemurian Dongyuemiao Member from previous studies, in which it is characterized by lacustrine limestones. However, similar to the Zhenzhuchong Member, reddish mudrocks and newly-interpreted calcisols indicate drier climate (Figs. 4 and 7 and Table S2). Calcretes within reddish mudrocks were reported at Dafang (Location A8. Zhang et al., 2016), Tianzhu (Location A9. Li and Chen, 2010), and Yunyang (Location A15. Meng et al., 2005) in the central and southern GSB (Figs 4 and 7). The probable calcisols indicate the (semi-) arid climate may have interrupted the long-term warm and (semi-) humid climate interpreted based on flora in the Early Jurassic (e.g., Meng et al., 1997; Li and Meng, 2003). This interpretation of (semi-) arid punctuation is also supported by the floral changes (Meng et al., 1997; Li and Meng, 2003) and geochemistry of mudrocks (Guo et al., 2017).

Few records of coeval terrestrial climate are known from other continents or regions in the literature. A report occurs in eastern England, where the co-occurrence of the acmes of thermophilic pollens *Classopollis classoides* and *Liasidium variabile* indicates the warm-humid climate in the late Sinemurian (Riding et al., 2013). The Whitmore Point Member of the Moenave Fm deposited in dryland lakes (Tanner and Lucas, 2008) and the upper part of eolian Navajo Sandstone (Blakey et al., 1988) could represent the coevally similar climate in Colorado Plateau although relatively cool (~9 to 18 ºC) continental climate was inferred from oxygen and hydrogen isotope composition of chert precipitated in interdune, freshwater lakes in the Navajo Sandstone (Kenny, 2015).

3) The Pliensbachian Age

The Ma'anshan Member is likely the Pliensbachian, though age information is lacking. In comparison to the previous member, the Ma'anshan Member diaplays a prominent change in the distribution extent of red color sediment and pedogenesis. The reddish sediments extend through the entire member (comp. Figs. 6 and S2) and can be observed across the GSB. Calcisols are documented in both the western and central GSB (Figs. 6, 7, S1, and S2). Ten calcisol horizons were recognized at the Shaping section, Ya'an (Figs. 6 and S1), and strong leaching structure and mudcrack are seen in Bed H8 of the Tanba section, Hechuan (Fig. 3a and 3d). Other more abundant calcretes within terrestrial red mudrocks were widely described at the Gaoxian section of Dafang (Location A8. Zhang et al., 2016), the Hulukou section of Weiyuan (Location A10. SBG, 1980a), the Geyaoguan section of Gulin (Location A13. SBG, 1976), the Taiyuan section of Fengdu (Location A16. SBG, 1975), and the Yaxi section of Zunyi (Location A17. Yang, 2015). We interpret these calcretes were formed by pedogenesis. The widespread distribution of redbeds and calcisols (Figs. 4 and 7) implies a (semi-) arid climate had been intensified in the GSB during the Pliensbachian age.

Plant and sporopollen fossils also indicate a change to drier climate in the Pliensbachian. With comparison to the Zhenzhuchong and Dongyuemiao Members, much fewer plant fossils were reported in this member (e.g., Meng and Chen, 1997; Wang et al, 2010), likely implying a rapid climatic change. The Pliensbachian-Toarcian sporopollen assemblages are dominated by classical sporomorph genera (*Dictyophyllidites- Cyathidites- Classopollis*), in which the dry-type gymnosperm spore *Classopollis* is more prevalent than in the Hettangian-Sinemurian (Zhang and Meng, 1987), also indicating the intensification of arid climate.

Similar dry temperate / subtropical climate was verified by the upland coniferous forest in Qaidam Basin, Northwest China (Wang et al., 2005). However, at the same time, it was the probably coolest / most humid climate in South Kazakhstan, central Asia (Tramoy et al., 2016). These discrepancies might corroborate the unstable and heterogeneous climate in the mid-latitude area of North Hemisphere in the Pliensbachian. In other hand, interdune playa mudstones of the Kayenta Fm (e.g., Bromley, 1992) indicate similar arid climate in Colorado Plateau, western America.

4) The Toarcian Age

In spite the fact that the Da'anzhai Member was deposited in the largest lacustrine transgression period (details see Appedix 1), climate-sensitive facies and stable isotoic geochemistry indicate that aridification could be the most intensive in the late Early Jurassic in the GSB.

Redbeds with abundant calcretes are well developed in the Da'anzhai Member (Figs. 4 and 7). Four calcisols horizons in the Shaping section, Ya'an (Figs. 6 and S1) and the leaching structure (Bed H13) in the Tanba section, Hechuan (Fig. 3c), were observed. Calcretes at sections of Dafang (Location A8. Zhang et al., 2016), Nanxi (Location A11. SBG 1980a), Gongxian (Location A12. Liang et al., 2006), and Yunyang (Location A15. Meng et al., 2005), also record the occurrence of calcisols. The widespread occurance of calcisols reveals that subaerial exposure of sediments often interrupted the lake environment, illustrating dynamic lake level fluctuations and aridification.

In addition to redbeds and calcisols, gypsum and micritic dolomites (SBG, 1980a; Mo and Yu, 1987; Peng, 2009; and this work) were reported in the western and southern GSB (Figs. 1, 4, and 7). It is plausible that gypsum and dolomites indicate arid climate type. Thoguh dolomites have been in dispute for the significance of climate due to great deal of diagenetic dolomites in deep time, a high abundance of dolomite was interpreted to form during greenhouse periods, characterized by warm climates, probably reflecting favourable conditions for evaporite deposition and dolomitization via hypersaline reflux (Warren, 2000). Dolomites are aslo thought the results of interplay of climate and sea-level / base-level change (e.g., Newport et al., 2017) or are interacted with climatic regimes (Vandeginste et al., 2012). So, the widespread micritic dolomites in the Da'anzhai Fm, associated with gypsum (Fig. 3f), can serve the determination of climate and suggest an arid climate. Gypsum occasionally occurs at Maliuping of Hechuan (Fig. 3f) and Wujiaba of Zigong (SBG, 1980a) , implying a short-term evaporitic climate in the central GSB.

Carbon and oxygen isotopes of lacustrine carbonates further support the aird climate in the Toarcian age in the GSB. In general, -9.0‰ to -3.0‰ of $\delta^{13}C$ and $\delta^{18}O$ values represent a range of normal river-lake and groundwater carbonates (Alonso-Zarza, 2003). Therefore, the mainly positive $\delta^{13}C$ values 0 to 2 ‰ (Fig. 5) from Hechuan (Wang et al., 2006) indicate the lakes were brackish or even saline, and the relatively heavy negative $\delta^{13}C$ values -1‰ to -3.5 ‰ (Fig. 5) from Zigong (Wang et al. 2006) and Ya'an (this work) denote low depletions of ^{13}C during calcite/aragonite precipitation and mean that the lakes were possibly brackish. In other hand, lightly negative $\delta^{18}O$ values -5‰ to -12 ‰ (Fig. 5) dominate the lacustrine carbonates, suggesting that closed lacustrine, palustrine and pond systems formed in a regional arid-semiarid climate with significant evaporation relative to precipitation.

The covariance of $\delta^{13}C$ and $\delta^{18}O$ is also a criterion to distinguish closed or open lakes (e.g., Talbot, 1990; Li and Ku, 1997).

That is, high $\delta^{18}O$ and low $\delta^{13}C$ values will be produced in relatively low temperature lake water when the covariation is negative; high values of both $\delta^{18}O$ and $\delta^{13}C$ will be produced in high-temperature meteoric water and indicate increased evaporation when the covariation is positive. Pronounced positive covariances (R^2=0.44-0.96) between carbon and oxygen isotopes (Fig. 5) indicate a typical arid-semiarid pattern of lakes in the central and western GSB.

The Da'anzhai Member has the same palynofloral assemblage with the Ma'anshan Member, in which the dry-type gymnosperm spore *Classopollis* is much more than in previous strata (e.g., Zhang and Meng, 1987; Wang et al., 2010), supporting the aridification indicated by climate–sensitive sediments and stable isotope ratios of lacustrine carbonates aforementioned.

Coastal Cheirolepidiacean (gymnosperm) forests indicate (temperate to subtropical) warm-humid climate punctuated by locally dry and/or arid events in the Toarcian in Qaidam Basin, Northwest China (Wang et al., 2005). In Inner Mongolia of North China, the thermophilous plants such as the dipteridaceous fern *Hausmannia*, bennettitales *Ptilophyllum*, display similar warm and humid climate interrupted by hot and even arid conditions in a short intervals of the Toarcian (Deng et al., 2017). The warm-wet climate was also indicated by assemblages of sporomorph and vegetation in the late Early Jurassic in Jurong of Jiangsu, Lower Yangtze area (Huang et al., 2000). In South Kazakhstan, central Asia, paleoflora and δ^2H values suggest slightly less humid and warmer conditions starting from the early Toarcian (Tramoy et al., 2016).

In summary, climate–sensitive sediments, carbon-oxygen isotope values and covariance, and palynoflora, together indicate that an overall (semi-) arid climate dominated the GSB during the Early Jurassic, possibly accompanied by occasional evaporitic climate. Relatively abundant calcisols suggest that the GSB was in a subtropical arid zone based on the paleoclimatic zonation model of paleosols (Mack and James, 1994) during the middle-late Early Jurassic. Through the Early Jurassic, this (semi-) arid climate in GSB is thoroughly comparable with the simultaneous arid climate recorded in dryland lacustrine and eolian facies in Colorado Plateau, western America (e.g., Blakey et al., 1988; Bromley, 1992; Tanner and Lucas, 2008; Parrish et al., 2017), but distinct from the relatively warm-humid climate indicated by sedimentological and floral characteristics in North China (e.g., Wang et al., 2005, Deng et al., 2017) and in the northern margin of Gondwanaland, relatively high latitudes of Southern Hemisphere (Jansson et al., 2008; Pole, 2009).

5.2. *p*CO_2 perturbations and events

Pedogenic carbonates found in various continental settings precipitate in direct contact with soil atmosphere and bed rock and hold a meaningful signature of past climate (Alonso-Zarza and Tanner, 2006). Ancient *p*CO_2 has been estimated by carbon isotope of pedogenic carbonates using the empirical (Cerling, 1991) and optimized (Ekart et al., 1999) formula. This paleosol method has roughly been applying in the Phanerozoic *p*CO_2 estimate (e.g., Cerling, 1991; Ekart et al., 1999; Retallack, 2001a) with >10 Myr interval of age resolution. There are few high age resolution *p*CO_2 reconstructions for the Early Jurassic. The focus on *p*CO_2 estimates has on the event horizons, such as the transition of the Triassic to Jurassic (e.g.,

https://doi.org/10.5194/cp-2020-35
Preprint. Discussion started: 13 May 2020

Tanner et al., 2001; Schaller et al., 2011). Herein we present the pCO_2 estimate in ~1.0 Myr age resolution of the Early Jurassic (Figs. 6 and 8c).

5.2.1. pCO_2 perturbation

Results of model estimates show that the pCO_2 values range 980-2610 ppmV with a mean 1660 ppmV in the Early Jurassic except for the Hettangian and can be divided into three intervals (Figs. 6 and 8c): phase I, stable 1500-2000 (mean ~1700) ppmV in the Zhenzhuchong and Dongyuemiao Members (Sinemurian age); phase II, main 1000-1500 (mean ~ 1300) ppmV in the Ma'anshan Members (Pliensbachian age); and phase III, great fluctuation 1094-2610 (mean ~1980) ppmV in the lower Da'anzhai Member (early Toarcian age).

The evolution and level of pCO_2 estimated by carbon isotope ratios of the pedogenic carbonates from the GSB are roughly comparable with the global composite based on the plant stomata method (data of the composite curve see Table S6), but difficult to compare to the global composite pCO_2 based on paleosols (Fig. 8c. Suchecki et al., 1988; Cerling, 1991; Ekart et al., 1999), which may be attributed to the shortage of global data and large age uncertainties (Table S5 and S6).

On the other hand, the swing of the pCO_2 has a similar pattern to coeval seawater temperature through the Early Jurassic although there are some discrepancies in pace (comp. Fig. 8b and 8c). That is, the relatively high pCO_2 1500-2000 ppmV approximately corresponds to the relatively high seawater mean temperature -2ºC to +2ºC in the Sinemurian age (Fig. 8b), low pCO_2 1000-1500 ppmV to low seawater mean temperature -5ºC to -2ºC in the Pliensbachian age (Fig. 8b), and quick rising pCO_2 of 1200 ppmV to ~2500 ppmV to the rapidly increased seawater temperature of -4ºC to +4ºC in the late Pliensbachian-early Toarcian (Fig. 8b). The pCO_2 record and the carbon isotope of the marine carbonates are also somewhat comparable (comp. Fig. 8a and 8c).

It has been disputed whether climate change was resulted from pCO_2 perturbation in the Phanerozoic (e.g., Veizer et al., 2000; Crowley and Berner, 2001; Royer, 2006). For instance, the pCO_2 has a strong control over global temperatures for much of the Phanerozoic (e.g., Crowley and Berner, 2001; Royer, 2006; Price et al., 2013; Mills et al., 2019), but a decoupling of CO_2 and temperature has also been suggested (e.g., Veizer et al., 2000; Dera et al., 2011; Schaller et al., 2011; Kashiwagi, 2016). The pattern of the Early Jurassic pCO_2 reconstructed from the carbon isotope of pedogenic carbonates in GSB, Southwest China, supports the coupling relationship of CO_2-temperature at a ~1.0 Myr resolution scale. Even so, models of the coupling and decoupling of CO_2-temperature have to consider: 1), age order of CO_2-temperature relevance, i.e. they should be related in the same age (long term or short term) hierarchy; 2) precise age constrain of individual CO_2 and temperature data; 3) methods of CO_2 and temperature estimates, depending on precondition, presumptions, parameters, uncertainty, sample diagenesis, etc.; 4) controls or influences of key factors such ice sheet, tectonic, paleogeography, cosmic ray flux, biota, volcanic eruption, and so on.

https://doi.org/10.5194/cp-2020-35
Preprint. Discussion started: 13 May 2020

5.2.2. Rapid pCO_2 falling events

The recovered Early Jurassic pCO_2 curve reveals two rapid falling events (Fig. 6 and 8c). The first event ($1E_{CO2}$) shows a quick drop from ~2370 ppmV (sample J1z-08-01 at depth 84.7 m) to 1350 ppmV (sample J1z-10-02 at depth 94.4 m) near the boundary of the Dongyuemiao and Ma'anshan Members (Fig. 6), or to 1075 ppmV (sample J1z-11-02 at depth 111.7 m), which took place in the early Pliensbachian (~190.4-189.9/189.1 Ma. Fig. 8c). The extent of the rapid falling pCO_2 is ~1000-1300 ppmV in 9.7-17.0 m. In other words, ~1000 ppmV drop could be accomplished within ~0.5-1.0 Myr based on the estimate of the rate of sediment deposition (Table S4).

While the corresponding early Pliensbachian climatic and isotopic-shifting events cannot be observed in the smoothed curves of the Early Jurassic seawater temperature and carbon cycle (Dera et al. 2011), the rapid falling event $1E_{CO2}$ is well correlated to the nearly coeval excursion events of carbon-oxygen isotopes recorded in western Tethys (Fig. 8). The $1E_{CO2}$ compares well to: 1) the rapid carbon isotope negative excursion of (oysters, belemnites, and brachiopods) shells from the Cleveland Basin, UK (Korte and Hesselbo, 2011) and northwest Algeria (Baghli et al., 2020), 2) that of organic matter and marine carbonates from southern Pairs Basin (Bougeault et al., 2017; Peti, et al., 2017), and 3) rapid oxygen isotope negative excursion (seawater warming) of belemnites from northern Spain (van de Schootbrugge et al., 2005). The rapid change of the stable isotope record had been called the Sinemurian-Pliensbachian boundary event (SPBE) and dated in the ammonite of the upper *Raricostatum* - lower *Jamesoni* zones (Bougeault et al., 2017).

The second event $2E_{CO2}$ displays a large drop of 2574 ppmV (sample J1z-18-01 at depth 252.7 m) to 1094 ppmV (sample J1z-19-01 at depth 272.3 m), ~1500 ppmV decrease within 19.6 m (estimated age interval ~0.8 Myr. Table S4 and Fig. 8c). Following the second drop, pCO_2 rises rapidly by ~1300 ppmV of 1094 ppmV to 2386 ppmV (sample J1Z-20-01 at depth 294.3 m) although only a few samples support the this cycle of pCO_2 falling-rising.

Strata in western Sichuan (Xu et al., 2017), may correlate to the time interval of the T-OAE, during which pCO_2 doubled over background values, from ~1000 ppmV to ~2000 ppmV (e.g., Beerling and Royer, 2002; McElwain et al., 2005; Berner, 2006). Given the chronostratigraphical correlation is challenging, the pCO_2 falling-rising cycle might correspond to the quick shifting cycle of stable isotopes during the T-OAE (Fig. 8b and 8c). In detail, the rapid falling-rising of pCO_2 is consistent with: 1) the quick negative-positive carbon isotope excursion of marine carbonates from Italy (Jenkyns and Clayton, 1986; Sabatino et al., 2009), England and Wales (Jenkyns and Clayton, 1997), north Spain (van de Schootbrugge et al., 2005), the Lusitanian Basin of Portugal (Hesselbo et al., 2007), Paris Basin (Hermoso et al., 2009), and Morocco (Bodin et al., 2016); 2) that of invertebrate calcareous shells from the Cleveland Basin of UK (Korte and Hesselbo, 2011) and northwest Algeria (Baghli et al., 2020); 3) that of marine organic matter from Morocco (Bodin et al., 2016), Yorkshire of England (Cohen et al., 2004; Kemp et al, 2005), Cardigan Bay Basin of UK (Xu et al., 2018), northern Germany (van de Schootbrugge et al., 2013), Alberta and British Columbia of Canada (Them II et al., 2017), northern Tibet of China (Fu et al.,

https://doi.org/10.5194/cp-2020-35
Preprint. Discussion started: 13 May 2020

Climate of the Past
Discussions

2016), and Japan (Izumi et al., 2018); 4) that of terrestrial organic matter from Sichuan Basin, China (Xu et al., 2017); and 5) quick oxygen isotope negative-positive shifting (seawater warming) of brachiopods (Suan et al., 2008) and fossil wood (Hesselbo et al., 2007) from the Lusitanian Basin, Portugal.

Multiple hypotheses have been proposed to interpret the 5°–6 °C decrease of sea surface temperatures in the late Pliensbachian (Bailey et al., 2003; van de Schootbrugge et al., 2005; Suan et al., 2010) and warming ~8 °C in the early Toarcian (Bailey et al., 2003; Suan et al., 2010), such as the sea level falling and rising (Hallam, 1978; Hesselbo and Jenkyns, 1998), methane release (e.g., Hesselbo et al., 2000; Kemp et al, 2005; Hermoso et al., 2009; Them II et al., 2017), and the Karoo–Ferrar eruptions (e.g., Hesselbo et al., 2000; Beerling and Brentnall, 2007; Bodin et al., 2016). Perhaps, these hypotheses somewhat explain the rapid change of sea surface temperatures, but it remains unclear how link the hypotheses to drastic falling of $p\mathrm{CO_2}$ in a high age resolution.

To sum up, the perturbation and rapid falling events of the Early Jurassic $p\mathrm{CO_2}$ values estimated from the carbon isotope of pedogenic carbonates in the GSB, are compatible with the response of stable isotopes and seawater temperature from coeval marine sediments. Whatever caused the rapid variations of sea surface temperatures, stable isotopes, and $p\mathrm{CO_2}$, their concordance implies that it is a positive feedback of the sea surface temperature to $p\mathrm{CO_2}$ through the Early Jurassic; accordingly, positive linkage could have taken place between the Early Jurassic climate and $p\mathrm{CO_2}$.

6. Conclusions

Based on analyses of climate-sensitive sediments and stable isotopes of the GSB, leading to a reconstruction of paleoclimate and $p\mathrm{CO_2}$, we conclude:

1) Climate–sensitive sediments and carbon-oxygen isotope values and covariances with palynofloral reference indicate that an overall warm-hot and (semi-) arid climate dominated the GSB during the Early Jurassic, possibly accompanied by occasional evaporitic climate in the Toarcian. This (semi-) arid climate in GSB is comparable with that in Colorado Plateau, western America, but distinct from the relatively warm-humid terrestrial climate recognized in other places of Chinese mainland (e.g., Qaidam, Inner Mongolia, and Lower Yangtze) and the northern Gondwanaland, relatively high latitudes of Southern Hemisphere,.

2) The Early Jurassic $p\mathrm{CO_2}$ values estimated from the carbon isotope of pedogenic carbonates in GSB show that a range between 980 ppmV and 2610 ppmV is ~3.5-10 times the pre-industrial value 275 ppmV and the mean 1720 ppmV is ~6 times the pre-industrial value.

3) Three phases of $p\mathrm{CO_2}$ values were distinguished: 1500-2000 (mean ~1700) ppmV in the Sinemurian age, 1000-1500 (mean ~ 1300) ppmV in the Pliensbachian age, and 1094-2610 (mean ~1980) ppmV in the early Toarcian. The phases manifest the perturbation of pCO2 in the Early Jurassic.

4) Two events of rapidly falling pCO_2 were also recognized: ~1000-1300 ppmV drop at the Sinemurian-Pliensbachian boundary and quick falling (-rising) by ~1500 ppmV in the early Toarcian. The rapid falling events of pCO_2 are compatible with the response of stable isotopes and seawater temperature from the coeval marine sediments, implying a positive feedback of climate to pCO_2 during the Early Jurassic.

Acknowledgements

We thank reviewers xxx xxx for constructive comments and suggestions. It is acknowledged this research was supported by Natural Science Foundation of China (NSFC) project 41672097.

References

Alonso-Zarza, A M. and Tanner, L. H.: Preface. Geol. Soc. Am. Spe. Pap., 416, v-vii, doi, 10.1130/0-8137-2416-3.v, 2006.

Alonso-Zarza, A. M.: Palaeoenvironmental significance of palustrine carbonates and calcretes in the geological record. Earth Sci. Rev., 60, 261-298, 2003.

Arabas, A., Schlogl, J., and Meiste C.: Early Jurassic carbon and oxygen isotope records and seawater temperature variations: Insights from marine carbonate and belemnite rostra (Pieniny Klippen Belt, Carpathians), Palaeogeogr. Palaeoclimatol. Palaeoecol., 485, 119–135, 2017

Baghli, H., Mattioli, E., Spangenberg, J. E., Bensalah, M., Arnaud-Godet, F., Pittet, B., and Suan, G.: Early Jurassic climatic trends in the south-Tethyan margin. Gondwana. Res., 77, 67-81, doi, 10.1016/j.gr.2019.06.016, 2019.

Bailey, T. R., Rosenthal, Y., McArthur, J. M., van de Schootbrugge, B., and Thirlwall, M. F.: Paleoceanographic changes of the Late Pliensbachian-Early Toarcian interval: a possible link to the genesis of an Oceanic Anoxic Event, Earth Planet. Sci. Lett., 212, 307-320, 2003.

Beerling, D. J. and Brentnall, S. J.: Numerical evaluation of mechanisms driving Early Jurassic changes in global carbon cycling, Geology, 5, 247–250, 2007.

Beerling, D. J. and Royer, D. L.: Reading a CO_2 signal from fossil stomata, The New Phytologist, 153, 387-397, doi:0. 1046/j. 0028-646X. 2001. 00335. x, 2002.

Berner, R. A.: GEOCARBSULF: A combined model for Phanerozoic atmospheric O_2 and CO_2, Geochi. Cosmochi. Ac., 70(23 Spec. Iss.), 5653-5664, 2006.

Blakey, R. C., Peterson, F., and Kocurek, G.: Synthesis of late Paleozoic and Mesozoic eolian deposits of the Western Interior of the United States, Sediment. Geol., 56, 3-125, doi, https://doi.org/10.1016/0037-0738(88)90050-4, 1988.

Bodin, S., Krencker, F. N., Kothe, T., Hoffmann, R., Mattioli, E., Heimhofer, U., and Kabiri, L.: Perturbation of the carbon cycle during the late Pliensbachian – early Toarcian: New insight from high-resolution carbon isotope records in

Morocco, J Afri. Earth Sci., 116, 89–104, doi, 10.1016/j.jafrearsci.2015.12.018, 2016.

Bougeault, C., Pellenard, P., Deconninck, J. F., Hesselbo, S. P., Dommergues, J. L:, Bruenau, L., Cocquerez, T., Laffont, R., Huret, E., and Thibault, N.: Climatic and palaeoceanographic changes during the Pliensbachian (Early Jurassic) inferred from clay mineralogy and stable isotope (C-O) geochemistry (NW Europe), Global Planet. Change, 149, 139-152, 2017.

Breecker, D. O., Sharp, Z. D., and McFadden, L. D.: Seasonal bias in the formation and stable isotope composition of pedogenic carbonate in modern soil from central New Mexico, USA, Geol. Soc. Am. Bull., 12, 630-640, 2010.

Bromley, M.: Topographic inversion of early interdune deposits, Navajo Sandstone (Lower Jurassic), Colorado Plateau, USA, Sediment. Geol., 80, 1-25, 1992.

Cerling, T. E.: Carbon dioxide in the atmosphere: evidence from Cenozoic and Mesozoic paleosols: Am. J. Sci., 291, 377-400, 1991.

Cerling, T. E.: Stable carbon isotopes in palaeosol carbonates, in: Palaeoweathering, palaeosurfaces and related continental deposits, edited by: Thiry, M. and Simm-CoinÇon, R., Spec. P Intl. Asso. Sedi., 27, 43-60, 1999.

Chandler, M. A., Rind, D., and Ruedy, R.: Pangaean climate during the Early Jurassic: GCM simulations and the sedimentary record of paleoclimate, Geol. Soc. Am. Bull., 104, 543–559, 1992.

Cheng, L. X., Chen, H. D., and Guo, Y.: Fan delta sedimentary facies and reservoir characteristics of Lower Jurassic Zhenzhuchong segment in Yuanba area, Northeast Sichuan, China, J Chengdu Uni. Technol. (Sci. Technol. Ed), 41(3), 283-292, 2014 (in Chinese with English abstract).

Cohen, A. S., Coe, A. L., Harding, S. M., and Schwark, L.: Osmium isotope evidence for the regulation of atmospheric CO_2 by continental weathering, Geology, 32, 157–160, 2004.

Crowley, T. J. and Berner, R. A.: CO_2 and climate change, Science, 292, 870–872, 2001.

Deng, S. H., Zhao, Y., Lu, Y. Z., Shang, P., Fan, R,, Li, X., Dong, S. X., and Liu, L.: Plant fossils from the Lower Jurassic coal-bearing formation of central InnerMongolia of China and their implications for palaeoclimate, Palaeoworld, 26: 279-316, 2017

Dera, G., Brigaud, B., Monna, F., Laffont, R., Pucéat, E., Deconinck, J. F., Pellenard P., Joachimski, M. M., and Durlet, C.: Climatic ups and downs in a disturbed Jurassic world, Geology, 39(3), 215-218, 2011.

Dong, Z. M.: A new prosauropod from Ziliujing Formation of Sichuan Basin, Verte. Palasiatica, 22(4), 310-313, 1984 (in Chinese with English abstract).

Duan, S. Y. and Chen, Y.: Mesozoic fossil plants and coal formation of eastern Sichuan Basin, in: Continental Mesozoic Stratigraphy and Paleontology in Sichuan Basin of China: Part II, Paleontological Professional Papers, People's Publ. House Sichuan, Chengdu, 491-519, 1982 (in Chinese).

Ekart, D. D., Cerling, T. E., Montñez, I. P., and Tabor, N. J.: A 400 million year carbon isotope record of pedogenic

https://doi.org/10.5194/cp-2020-35
Preprint. Discussion started: 13 May 2020

carbonate: implications for paleoatmospheric carbon dioxide, Am. J. Sci., 299, 805-827, 1999.

Flügel, E.: Microfacies of Carbonate Rocks: Analysis, Interpretation and Application, Springer-Verlag, Berlin, Heidelberg, New York, 976 pp. 2004.

Fu, X. G., Wang, J., Feng, X. L., Wang, D., Chen, W. B., Song, C. Y., and Zeng, S. Q.: Early Jurassic carbon-isotope excursion in the Qiangtang Basin (Tibet), the eastern Tethys: implications for the Toarcian Oceanic anoxic event, Chem. Geol., 442, 67–72, 2016.

Gómez, J. J., Comas-Rengifo, M. J., and Goy, A.: Palaeoclimatic oscillations in the Pliensbachian (Early Jurassic) of the Asturian Basin (Northern Spain), Clim. Past, 12, 1199-1214, 2016.

Gómez, J. J., Goy, A., and Canales, M. L.: Seawater temperature and carbon isotope variations 15 in belemnites linked to mass extinction during the Toarcian (Early Jurassic) in Central and Northern Spain. Comparison with other European sections, Palaeogeogr. Palaeoclimatol. Palaeoecol., 258, 28-58, 2008.

Guo, L. Y., Zhang, S. W., Xie, X. N., Li, Z. S., Huang, C. Y., and Chen, B. C.: Geochemical characteristics and organic matter enrichment of the Dongyuemiao Member mudstone of Lower Jurassic in the Western Hubei-Eastern Chongqing, Ear. Sci., 42(7): 1235-1246, 2017 (in Chinese with English abstract).

Guo, X. S., Hu, D. F., Li, Y. P., Wei, X. F., Liu, R. B., Liu, Z. J., Yan, J. H., and Wan, Q. B.: Analyses and thoughts on accumulation mechanisms of marine and lacustrine shale gas: A case study in shales of Longmaxi Formation and Da'anzhai Section of Ziliujing Formation in Sichuan Basin, Ear. Sci. Front., 23(2), 18-28, 2016, (in Chinese with English abstract).

Guo, Z. W, Deng, K. L., and Han, Y. H.: Formation and Evolution of the Sichuan Basin, Geo. Publ. House, Beijing, 200, 1996.

Hallam, A.: Eustatic cycles in the Jurassic, Paleogeogr. Paleoclimatol. Paleoecol., 23, 1-32, 1978.

He, T. H. and Liao, C. F.: Control of Upper Triassic division and correlation and Indosinian Movement on oil and gas accumulation in Sichuan Basin, Acta Geol. Sichuan, 00, 40–55, 1985 (in Chinese).

Hermoso, M., Le Callonnec, L., Minoletti, F., Renard, M., and Hesselbo, S. P.: Expression of the Early Toarcian negative carbon-isotope excursion in separated carbonate microfractions (Jurassic, Paris Basin), Earth Planet. Sci. Lett., 277, 194-203, 2009.

Hesselbo, S. P. and Jenkyns, H. C.: British Lower Jurassic sequence stratigraphy, in: Mesozoic-Cenozoic Sequence Stratigraphy of European Basins, edited by: de Graciansky, P. C., Hardenbol, J., Jacquin, Th., and Vail, P. R., SEPM Spec. Pap., 60, 562-581, 1998.

Hesselbo, S. P., Bjerrum, C. J., Hinnov, L. A., MacNiocaill, C., Miller, K. G., Riding, J. B., van de Schootbrugge, B., and the Mochras Revisited Science Team: Mochras borehole revisited: a new global standard for Early Jurassic earth history, Sci. Dril., 16, 81–91. doi:10. 5194/sd-16-81-2013, 2013.

https://doi.org/10.5194/cp-2020-35
Preprint. Discussion started: 13 May 2020

Climate of the Past
Discussions

Hesselbo, S. P., Gröcke, D. R., Jenkyns, H. C., Bjerrum, C. J., Farrimond, P., Morgans Bell, H. S., Green, O. R.: Massive dissociation of gas hydrate during a Jurassic oceanic anoxic event, Nature, 406, 392-395, doi:10. 1038/35019044., 2000.

Hesselbo, S. P., Jenkyns, H. C., Duarte, L. V., and Oliveira, L. C. V.: Carbon-isotope record of the Early Jurassic (Toarcian) Oceanic Anoxic Event from fossil wood and marine carbonate Lusitanian Basin, Portugal, Earth Planet. Sci. Lett., 253, 455-470, 2007.

Huang, P., Guan, Y. M., and Yang, X. Q.: Early Jurassic palynoflora from a drilling section of Jurong, Jiangsu, Acta Micropalaeontol. Sin., 17(1), 85- 98, 2000.

Huang, Q. S.: Paleoclimate and coal-forming characteristics of the Late Triassic Xujiahe stage in northern Sichuan, Geol. Rev., 41(1): 92–99, 1995, (in Chinese with English abstract).

Huang, Q. S.: The flora and paleoenvironment of the Early Jurassic Zhenzhuchong Formation in Daxian-Kaixian region, northern margin of the Sichuan Basin, Ear. Sci. ------ J. China Uni. Geosci., 3, 221-229, 2001 (in Chinese with English abstract).

Imbellone, P. A.: Classification of Paleosols. São Paulo, UNESP, Geociências, 30(1), 5-13, 2011,

Izumi, K., Kemp, D., Itamiya, S., and Inui, M.: Sedimentary evidence for enhanced hydrological cycling in response to rapid carbon release during the early Toarcian oceanic anoxic event, Earth Planet. Sci. Lett., 481, 162–170, 2018.

Jansson, I. M., McLoughlin, S., Vajda, V., and Pole, M.: An Early Jurassic flora from the Clarence-Moreton Basin, Australia, Rev. Palaeobot. Palyno., 150, 5–21, http://dx.doi.org/10.1016/j. revpalbo.2008.01.002, 2008.

Jenkyns, H. C. and Clayton, C. J.: Black shales and carbon isotopes in pelagic sediments from the Tethyan Lower Jurassic, Sedimentology, 33, 87-106, 1986.

Jenkyns, H. C., and Clayton, C. J., Lower Jurassic epicontinental carbonates and mudstones from England and Wales: chemostratigraphic signals and the early Toarcian anoxic event, Sedimentology, 44, 687-706, 1997.

Jenkyns, H. C., Jones, C. E., Gröcke, D. R., Hesselbo, S. P., and Parkinson, D. N.: Chemostratigraphy of the Jurassic System: Applications, limitations and implications for palaeoceanography, J. Geol. Soc. London, 159, 351-378, 2002.

Jenkyns, H. C.: Geochemistry of oceanic anoxic events, Geochem. Geophys. Geosyst., 11, Q03004. doi:10. 1029/2009GC002788, 2010.

Kashiwagi, H.: Atmospheric carbon dioxide and climate change since the Late Jurassic (150 Ma) derived from a global carbon cycle model, Palaeogeogr. Palaeoclimatol. Palaeoecol., 454, 82–90, 2016.

Kemp, D. B., Coe, A. L., Cohen, A. S., and Schwark, L.: Astronomical pacing of methane release in the Early Jurassic period, Nature, 437, 396-399, doi, org/10. 1038/nature04037, 2005.

Kenny, R.: A cool time in the Early Jurassic: first continental palaeoclimate estimates from oxygen and hydrogen isotope ratios in chert from Navajo Sandstone carbonate lenses, Utah (USA), Carbonate Evaporite, doi,

https://doi.org/10.5194/cp-2020-35
Preprint. Discussion started: 13 May 2020

10.1007/s13146-015-0276-z, 2015.

Kent, D. V., Olsen, P. E., and Muttoni, G.: Astrochronostratigraphic polarity time scale (APTS) for the Late Triassic and Early Jurassic from continental sediments and correlation with standard marine stages, Earth-Sci. Rev., 166, 153-180, 2017.

Korte, C., and Hesselbo, S. P.: Shallow marine carbon and oxygen isotope and elemental records indicate icehouse-greenhouse cycles during the Early Jurassic, Paleoceanography, 26, 1–18, 2011.

Korte, C., Hesselbo, S. P., Jenkyns, H. C., Rickaby, R. E. M., and Spötl, C.: Palaeoenvironmental significance of carbon- and oxygen-isotope stratigraphy of marine Triassic-Jurassic boundary sections in SW Britain, J. Geol. Soc. London, 166(3), 431-445, 2009.

Li, H. C. and Ku, T. L.: $\delta^{13}C$-$\delta^{18}O$ covariance as a paleohydrological indicator for closed basin lakes, Palaeogeogr. Palaeoclimatol. Palaeoecol., 133, 69-80, 1997.

Li, L. Q., Wang, Y. D., Liu, Z. S., Zhou, N., and Wang, Y.: Late Triassic palaeoclimate and palaeoecosystem variations inferred by palynological record in the northeastern Sichuan Basin, China, Paläontol. Zeits., 309-324, DOI 10. 1007/s12542-016-0309-5, 2016.

Li, W. M. and Chen, J. S.: Discovery and significances of the Jurassic Ziliujing Formation in Tianzhu, Guizhou, China New Techn. Prod., 13, 134-135, 2010 (in Chinese).

Li, X. B. and Meng, F. S.: Discovery of fossil plants from the Ziliujing Formation in Hechuan of Chongqing. Geol. Min. Resour. South China, 3: 60-65, 2003 (in Chinese with English abstract).

Li, X. H., Jenkyns, H. C., Zhang, C. K., Wang, Y., Liu, L., and Cao, K.: Carbon-isotope signatures of pedogenic carbonates from SE China: Rapid atmospheric pCO_2 changes in the mid–late Early Cretaceous, Geol. Mag. 151 (5), 830-849, doi:10. 1017/S0016756813000897, 2014.

Li, Y. Q. and He, D. F.: Evolution of tectonic-depositional environment and prototype basins of the Early Jurassic in Sichuan Basin and adjacent areas, Acta Petrol. Sin., 35(2), 219-232, 2014 (in Chinese with English abstract).

Li, Y., Allen, P. A., Densmore, A. L., and Xu, Q.: Evolution of the Longmen Shan Foreland Basin (Western Sichuan, China) during the Late Triassic Indosinian Orogeny. Basin Res., 15, 117-138, 2003.

Liang, B., Wang, Q. W., and Kan, Z. Z.: Geochemistry of Early Jurassic mudrocks from Ziliujing Formation and implications for source-area and weathering in dinosaur fossils site in Gongxian, Sichuan province, J. Min. Petr., 26(3), 94-99, 2006 (in Chinese with English abstract).

Liu, B. J. and Zeng, Y. F., eds.: Foundation and methodology of lithofacies and paleogeography, Geo. Publ. House, Beijing, 442, 1986 (in Chinese).

Liu, J. L., Ji, Y. L., Zhang, K. Y., Li, L. D., Wang, T. Y., Yang, Y., and Zhang, J.: Jurassic sedimentary system transition and evolution model in western Sichuan Foreland Basin, Acta Petrol. Sin., 37(6), 743-756, 2016 (in Chinese with

https://doi.org/10.5194/cp-2020-35
Preprint. Discussion started: 13 May 2020

English abstract).

Ma, Y. S., Chen, H. D., Wang, G. L., Guo, T. L., Tian, J. C., Liu, W. J., Xu, X. S., Zheng, R. C., Mou, C. L., and Hou, M. C.: Atlas of Lithofacies Paleogeography on the Sinian-Neogene Tectonic-Sequence in South China, Science Press, Beijing, 162-165, 2009 (in Chinese).

Mack, G. H. and James, W. C.: Paleoclimate and the Global Distriution of Paleosols, J. Geol., 102, 360-366, 1994.

Mack, G. H., James, W. C., and Monger, H. C.: 1 Classification of paleosols, Geol. Soc. Am. Bull., 105, 129–136, 1993.

McArthur, J. M., Donovan, D. T., Thirlwall, M. F., Fouke, B. W., and Mattey, D.: Strontium isotope profile of the early Toarcian (Jurassic) oceanic anoxic event, the duration of ammonite biozones, and belemnite palaeotemperatures, Earth Planet. Sci. Lett., 179, 269-285, 2000.

McElwain, J. C., Wade-Murphy, J., and Hesselbo, S. P.: Changes in carbon dioxide during an oceanic anoxic event linked to intrusion into Gondwana coals, Nature, 435, 479-482, doi:org/10. 1038/nature03618, 2005.

Meng, F. S. and Chen, D. Y.: Fossil plants and palaeoclimatic environment from the Ziliujing Formation in the western Yangtze Gorges area, China, Geol. Min. Resour. S. China, 1, 51-59, 1997 (in Chinese with English abstract).

Meng, F. S., Chen, H. M., and Li, X. B.: Study on Lower Middle Jurassic boundary in Chongqing region, Geol. Min. Resour. S China, 3, 64-71, 2005 (in Chinese with English abstract).

Meng, F. S., Li, X. B, and Chen, H. M.: Fossil plants from Dongyuemiao Member of the Ziliujing Formation and Lower-Middle Jurassic boundary in Sichuan basin, China, Acta Palaeontol. Sin., 42(4), 525-536, 2003. (in Chinese with English abstract).

Metodiev, L. and Koleva-Rekalova, E.: Stable isotope records (δ18O and δ13C) of Lower - Middle Jurassic belemnites from the Western Balkan mountains (Bulgaria), Palaeoenvironmental application, Appl. Geochem., 23, 2845–2856, 2008.

Mills B. J. W., Krause A. J., Scotese C. R., Hill D. J., Shields G. A., and Lenton T. M.: Modelling the long-term carbon cycle, atmospheric CO_2, and Earth surface temperature from late Neoproterozoic to present day, Gondwana Res., 67, 172–186, 2019.

Mo, Y. Z. and Yu, H. Y.: The discovery and its geological significance of dolomite in Ziliujing Groups of Middle and Lower Jurassic Series in Ma'anshan Member, Geol Guizhou, 10(1), 110-113, 1987 (in Chinese with English abstract).

Myers, T. S., Tabor, N. J., Jacobs, L. L., and Mateus, O.: Estimating soil $p\mathrm{CO}_2$ using paleosol carbonates: implications for the relationship between primary productivity and faunal richness in ancient terrestrial ecosystems, Paleobiology, 38(4), 585–604, 2012.

Newport, R., Hollis, C., Bodin, S., and Redfern, J.: Examining the interplay of climate and low amplitude sea-level change on the distribution and volume of massive dolomitization: Zebbag Formation, Cretaceous, Southern Tunisia, Deposit. Rec., 3(1), 38–59, doi,10.1002/dep2.25, 2017.

Nordt, L., Atchley, S., and Dworkin, S.: Terrestrial evidence for two greenhouse events in the latest Cretaceous, Geol. Soc.

https://doi.org/10.5194/cp-2020-35
Preprint. Discussion started: 13 May 2020

Am. Today, 13, 12, 4-9, doi, 10.1130/1052-5173(2003)013 <4, 2003.

Parrish, J. T., Hasiotis, S. T., and Chan, M. A.: Carbonate deposits in the Lower Jurassic Navajo Sandstone, southern Utah and northern Arizona, J. Sedi. Res., 87, 740-762, doi, https://doi.org/10.2110/jsr.2017.42, 2017.

Parrish, J. T., Rasbury, E. T., Chan, M. A., and Hasiotis, S. T.: Earliest Jurassic U-Pb ages from carbonate deposits in the Navajo Sandstone, southeastern Utah, USA, Geology, 47(11), 1015–1019, doi, 10.1130/g46338.1, 2019.

Peng, G. Z.: Assemblage characters of Jurassic dinosaurian fauna in Zigong of Sichuan, J. Geosci., 33(2), 113-123, 2009 (in Chinese with English abstract).

Peti, L., Thibault, N., Clémence, M. E., Korte, C., Dommergues, J. L., Bougeault, C., Pellenard,P., Jelby, M. E., and Ullmann, C. V.: Sinemurian-Pliensbachian Calcareous Nannofossil Biostratigraphy and Organic Carbon Isotope Stratigraphy in the Paris Basin: Calibration to the Ammonite Biozonation of NW Europe, Palaeogeogr. Palaeoclimatol. Palaeoecol., 468, 142–161, 2017.

Philippe M., Puijalon S., Suan G., Mousset S., Thévenard F., and Mattioli E.: The palaeolatitudinal distribution of fossil wood genera as a proxy for European Jurassic terrestrial climate, Palaeogeogr. Palaeoclimatol. Palaeoecol., 466, 373–381, 2017.

Pole, M.: Vegetation and climate of the New Zealand Jurassic, GFF, 131:1-2, 105-111, DOI: 10. 1080/11035890902808948, 2009.

Price, G. D., Twitchett, R. J., Wheeley, J. R., and Buono, G.: Isotopic evidence for long term warmth in the Mesozoic, Sci. Rep., 3, 1438, doi, 10.1038/srep01438, 2013.

Price, G. D.: The evidence and implications of polar ice during the Mesozoic, Earth-Sci. Rev., 48, 183-210, 1999.

Qian, T., Liu, S. F., Wang, Z. X., Li, W. P., and Chen, X. L.: Characteristics of the Baitianba Formation conglomerate of Lower Jurassic in the northern Sichuan basin and its constraint to the uplift of the south Dabashan, China Sci. Paper, 11(21), 2402-2408, 2016 (in Chinese with English abstract).

Rees, P. A., Zeigler, A. M., and Valdes, P. J.: Jurassic phytogeography and climates: new data and model comparisons, in: Warm Climates in Earth History, edited by: Huber, B., MacLeod, K., and Wing, S., Cambridge University Press, 297–318, 1999.

Retallack, G. J.: A 300-million-year record of atmospheric carbon dioxide from fossil plant cuticles, Nature, 411, 287-290, 2001a.

Retallack, G. J.: Adapting soil taxonomy for use with paleosols. Quatern. Int., 51/52: 55-57, doi, 10.1016/S1040-6182(98)00039-1, 1998.

Retallack, G. J.: Soils of the Past--An Introduction to Paleopedology, Blackwell Science Ltd, Oxford, 333, 2001b.

Riding, J. B., Leng, M. J., Kender, S, Hesselbo, S. P., and Feist-Burkhardt, S.: Isotopic and palynological evidence for a new Early Jurassic environmental perturbation, Palaeogeogr. Palaeoclimatol. Palaeoecol., 374,: 16–27, 2013.

https://doi.org/10.5194/cp-2020-35
Preprint. Discussion started: 13 May 2020

Climate of the Past Discussions
Open Access EGU

Rosales, I., Quesada, S., and Robles, S.: Primary and diagenetic isotopic signals in fossils and hemipelagic carbonates: the Lower Jurassic of northern Spain, Sedimentology, 48, 1149–1169, 2001.

Ros-Franch, S., Echevarría, J., Damborenea, S. E., Manceñido, M. O., Jenkynsb, H. C., Al-Suwaidi, A., Hesselbo, S. P., and Riccardi A. C.: Population response during an Oceanic Anoxic Event: The case of Posidonotis (Bivalvia) from the Lower Jurassic of the Neuquén Basin, Argentina, Palaeogeogr. Palaeoclimatol. Palaeoecol., 525, 57–67, 2019.

Royer, D. L.: CO_2-forced climate thresholds during the Phanerozoic: Geochi. Cosmochi. Ac., 70, 56, 65–75, doi: 10. 1016/j.gca.2005.11.031, 2006.

Sabatino, N., Neri, R., Bellanca, A., Jenkyns,H., Baudin, F., Parisi, G., and Maseti, D.: Carbon isotope records of the Early Jurassic (Toarcian) oceanic anoxic event from the Valdorbia (Umbria-Marche Apennines) and Monte Mangart (Julian Alps) sections: palaeogeographic and stratigraphic implications, Sedimentology, 56, 1307-1328, 2009.

SBG (Sichuan Bureau of Geology): Reports of 1:200,000 Regional Geology Investigations (Profile Qianjiang), 48, 1975 (in Chinese).

SBG (Sichuan Bureau of Geology): Reports of 1:200,000 Regional Geology Investigations (Profile Xuyong), 55, 1976 (in Chinese).

SBG (Sichuan Bureau of Geology): Reports of 1:200,000 Regional Geology Investigations (Profiles Suining, Zigong, Neijiang, Yibin, and Luzhou), 43-50,1980a (in Chinese).

SBG (Sichuan Bureau of Geology): Reports of 1:200,000 Regional Geology Investigations (Profiles Yilong, Tongjiang, Nanchong, Guang'an, and Chongqing), 100-101, 1980b (in Chinese).

SBGM (Sichuan Bureau of Geology and Mineral Resources): Geology of Sichuan Province, Geol. Publ. House, Beijing, 730, 1991 (in Chinese with English summary).

SBGM: Lithostratigraphy of Sichuan Province, China Uni. Geosci. Press, Wuhan, 388, 1997 (in Chinese).

Schaller, M. F., Wright, J. D., and Kent, D. V.: Atmospheric $p$$CO_2$ perturbations associated with the Central Atlantic Magmatic Province, Science, 331, 1404-1409, doi, 10.1126/science.1199011, 2011.

Selley, R. C.: Ancient Sedimentary Environments and their sub-surface diagnosis (fourth edition), Chapman & Hall, London, 296, 1996.

Sellwood, B. W., and Valdes, P. J.: Jurassic climates, P. Geologist Assoc., 119, 5-17, 2008.

Smoot, J. P. and Olsen, P. E.: Climatic cycles as sedimentary controls of rift basin lacustrine deposits in the early Mesozoic Newark basin based on continuous core, edited by Lomando, A. J. and Harris, M., Lacustrine Depositional Systems, SEPM Core Workshop Notes, 19, 201-237, 1994.

Soil survey Staff: Keys to Soil Taxonomy, Pocahontas Press, Blacksburg, VA, 1998.

Steinthorsdottir, M. and Vajda, V.: Early Jurassic (late Pliensbachian) CO_2 concentrations based 5 on stomatal analysis of fossil conifer leaves from eastern Australia, Gondwana Res. 27, 829-897, 2015.

Suan, G., Mattioli, E., Pittet, B., Lécuyer, C., Suchéras-Marx, B., Duarte, L. V., Philippe, M., Reggiani, L., and Martineau, F.: Secular environmental precursors to Early Toarcian (Jurassic) extreme climate changes, Earth Planet. Sci. Letts., 290, 448-458, doi, org/10. 016/j.epsl.2009.12.047, 2010.

Suan, G., Mattioli, E., Pittet, B., Mailliot, S., and Lécuyer, C.: Evidence for major environmental perturbation prior to and during the Toarcian (Early Jurassic) oceanic anoxic event from the Lusitanian Basin, Portugal, Paleoceanography, 23, PA1202, doi, org/10. 1029/2007PA001459, 2008.

Suchechi, R. K., Hubert, F. F., and Birney de Wet, C. C.: Isotopic imprint of climate and hydrogeochemistry on terrestrial strata of the Triassic-Jurassic Hartford and Fundy rift basins, J. Sediment. Petr., 58, 801-811, 1988.

Talbot, M. R.: A review of the palaeohydrological interpretation of carbon and oxygen isotopic ratios in primary lacustrine carbonates. Chem. Geol. (Isotope Geoscience Section), 80, 261-2791, 1990.

Tanner, L. H., and Lucas, S. The Whitmore Point Member of the Moenave Formation: Early Jurassic Dryland Lakes on the Colorado Plateau, Southwestern USA, Volum. Jur., 6(6), 11-21, 2008.

Tanner, L. H., Hubert, J. F., Coffey, B. P., and McInerney, D. P.: Stability of atmospheric CO_2 levels across the Triassic/Jurassic boundary, Nature, 411, 675-677, 2001.

Them, TR, II, Gill, B. C., Caruthers, A. H., Gröcke, D. R., Tulsky, E. T., Martindale, R. C., Poulton, T. P., and Smit, P. L.: High-resolution carbon isotope records of the Toarcian oceanic anoxic event (Early Jurassic) from North America and implications for the global drivers of the Toarcian carbon cycle, Earth Planet. Sci. Lett., 459, 118–126, 2017.

Tramoy, R., Schnyder, J., Nguyen, Tu T. T., Yans, J., Jacob, J., Sebilo, M., Derenne, S., Philippe, M., Huguet, A., Pons, D., and Baudin, F.: The Pliensbachian-Toarcian paleoclimate transition: New insights from organic geochemistry and C, H, N isotopes in a continental section from Central Asia, Palaeogeogr. Palaeoclimatol. Palaeoecol., 461, 310–327, 2016.

Tucker, M. E.: Sedimentary rocks in the field - a practical guide (4th ed.), Wiley-Blackwell, Chichester, England, 276 pp, 2011.

Vandeginste, V., and John, C. M.: Influence of climate and dolomite composition on dedolomitization: insights from a multi-proxy study in the central Oman Mountains, J. Sediment. Res., 82(3), 177-195, doi, 10.2110/jsr.2012.19, 2012.

van de Schootbrugge, B., Bailey, T. R., Katz, M. E., Wright, J. D., Rosenthal, Y., Feist-Burkhardt, S., and Falkowski, P. G.: Early Jurassic climate change and the radiation of organic walled phytoplankton in the Tethys Sea, Paleobiology, 31, 73–97, 2005.

Veizer, J., Godderis ,Y., and François, L. M.: Evidence for decoupling of atmospheric CO_2 and global climate during the Phanerozoic eon, Nature, 408, 698-701, 2000.

Wang, Q. W., Liang, B., Kan, Z. Z.: Carbon and oxygen isotopic compositions of lacustrine carbonates of the Early Jurassic Ziliujing Formation in the Sichuan Basin and their paleolimnological significance, J. Min. Petr., 26(2), 87-91, 2006 (in Chinese with English abstract).

Wang, Y. D., Fu, B. H., Xie, X. P., Huang, Q. S., Li, K., Liu, Z. S., Yu, J. X., Pan, Y. H., Tian, N., and Jiang, Z. K.: The Terrestrial Triassic and Jurassic Systems in the Sichuan Basin, China, in: Contributions to the 8th International Congress odd the Jurassic System, edited by: Sha, J. G., Shi, X. Y., Zhou, Z. H., Wang, Y. D., Uni. Sci. Techn., China Press, Hefei, Anhui, 1-136, 2010 (in Chinese).

Wang, Y. D., Mosbrugger, V., and Zhang, H.: Early to Middle Jurassic vegetation and climatic events in the Qaidam Basin, Northwest China, Palaeogeogr. Palaeoclimatol. Palaeoecol., 224, 200–216, http://dx.doi.org/10.1016/j.palaeo.2005.03.035, 2005.

Warren, J.: Dolomite: occurrence, evolution and economically important associations, Earth Sci. Rev., 52, 1–81, 2000.

Wei, M.: Continental Mesozoic Stratigraphy and Paleontology in the Sichuan Basin, People's Publ. House of Sichuan, Chengdu, 346-363, 1982 (in Chinese with English summary).

Wen, W. and Zhao, B.: Stratigraphic character and sedimentary facies of the Ziliujing Formation in the Pujiang-Ya'An area, Sichuan province, J. Stratigr., 34(2), 219-224, 2010 (in Chinese with English abstract).

Wright, V. P.: Paleosol Recognition: A guide to early diagenesis in terrestrial settings (Chapter 12), in: Developments in Sedimentology, edited by: Wolf K, H. and Chilingarian, G. V., 47, 591-619, 1992.

Xu, C. M, Gehenn, J. M., Zhao, D. H., Xie, G. Y., and Teng, M. K.: The fluvial and lacustrine sedimentary systems and stratigraphic correlation in the Upper Triassic Xujiahe Formation in Sichuan Basin, China, AAPG Bull., 99(11), 2023-2041, doi, 10. 1306/07061514236, 2015.

Xu, W. M, Ruhl, M., Jenkyns, H. C., Leng, M. J., Huggett, J. M., Minisini, D., Ullmann, C. V., Riding, J. B., Weijers, J. W. H., Storm, M. S., Percival, L. M. E., Tosca, N. J., Idiz, E. F., Tegelaar, E. W., Hesselbo, S. P.: Evolution of the Toarcian (Early Jurassic) carbon-cycle and global climatic controls on local sedimentary processes (Cardigan Bay Basin, UK), Earth Planet. Sci. Lett., 484, 396-411, 2018.

Xu, W. M., Ruhl, M., Jenkyns, H. C., Hesselbo. S. P., Riding, J. B., Selby, D., Naafs, B. D. A., Weijers, J. W. H., Pancost, R. D., Tegelaar, E. W., and Idiz, E. F.: Carbon sequestration in an expanded lake system during the Toarcian oceanic anoxic event, Nat. Geosci., 129-135, doi, 10. 1038/NGEO2871, 2017.

Yang, G. L.: Heavy mineral stratigraphy of Mesozoic continental clastic facies in Yaxi area, northern Guizhou, J. Stratigr., 39(1), 89-96 , 2015 (in Chinese with English abstract).

Yang, W., Zuo, R. S., Chen, D. X., Jiang, Z. X., Guo, L. S., Liu, Z. Y., Chen, R., Zhang, Y. P., Zhang, Z. Y., Song, Y., Luo, Q., Wang, Q. Y., Wang, J. B., Chen, L., Li, Y. H., Zhang, C.: Climate and tectonic-driven deposition of sandwiched continental shale units: New insights from petrology, geochemistry, and integrated provenance analyses (the western Sichuan subsiding Basin, Southwest China), Int. J. Coal Geol., 211,103-227, 2019.

Ye, M. N., Liu, X. Y., and Huang, G. Q.: Late Triassic and Early-Middle Jurassic fossil plants from northeastern Sichuan, Sci. Techn. Press. Hefei, Anhui, 1986 (in Chinese with English summary).

https://doi.org/10.5194/cp-2020-35
Preprint. Discussion started: 13 May 2020

Zhang, L. M., Wang, C. S , Wignall, P. B., Kluge, T., Wan, X. Q., Wang, Q., and Gao, Y.: Deccan volcanism caused coupled $p\mathrm{CO}_2$ and terrestrial temperature rises, and pre-impact extinctions in northern China, Geology, 46(3), 271-274, 2018.

Zhang, X. S., Zhao, B., Tan, M., Zhou, B. Y., Sun, J.: Stratigraphic Characteristics of Ziliujing Formation，Jurassic Series and Discovery of Dinosaur Footprints in Dafang,Guizhou, Geol. Guizhou, 33(1), 50-70, 2016 (in Chinese with English abstract).

Zhang, Z. L. and Meng, F. S.: Chapter 2, the Jurassic. In Zhang Zhenlai and Meng Fansong eds. The Triassic-Jurassic Biostratigraphy in Yangtze Gorges (4), Geol. Publ. House, Beijing, 408, 1987 (in Chinese with English summary).

https://doi.org/10.5194/cp-2020-35
Preprint. Discussion started: 13 May 2020

Climate of the Past
Discussions
Open Access

Figures

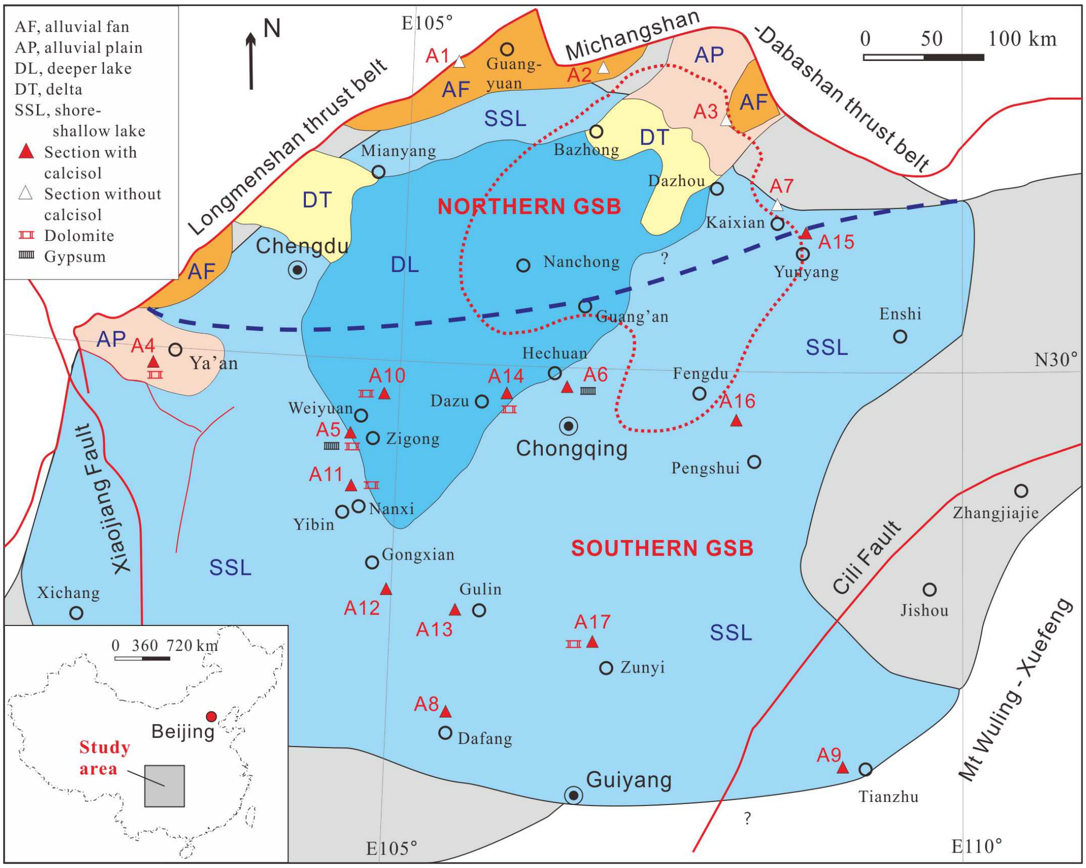

Figure 1 **Lithofacies paleogeographic sketch of the grand Sichuan paleobasin (GSB) in the early Early Jurassic (Zhenzhuchong and Dongyuemiao members) showing locations of the observed and analysed sections and climate-sensitve sediments. Lithofacies paleogeographic map was composed and modified from Ma et al. (2009) and Li and He (2014). Blue area is the extent of paleolake, estemted as ~380,000 km^2; blue + gray region is the basin shape, eitmated ~480,000 km^2. Dot red line confines the deeper lake area in the late Early Jurassic (Ma'anshan and Da'anzhai members). Bold dashed line is the northern edge of calcisol occurrence, which may separate the climate of the GSB as the northern and southern types. Triangles with numbers are locations of observed and analysed sections: A1, Xiasi section, Jian'ge; A2, Puji section, Wangcang; A3, Shiguansi section, Wanyuan; A4, Shaping section, Ya'an (bed and thickness from Wen and Zhao, 2010); A6, Tanba and Maliping section, Hechuan (bed and thickness from Wang et al., 2010); A7, Wenquan section, Kaixian (thickness from Wang et al., 2010). Location and source data s of sections A5 and A8-A17 (climate-sensitive sediments) refer to supplementary data Table S2.**

https://doi.org/10.5194/cp-2020-35
Preprint. Discussion started: 13 May 2020

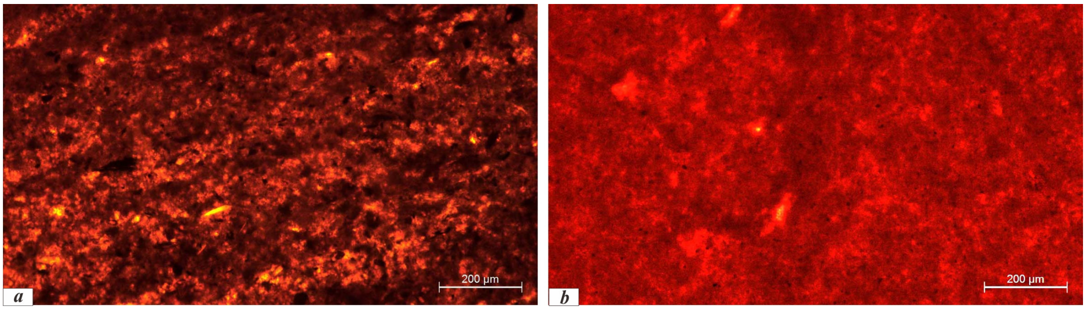

Figure 2 Microscopic cathodoluminescence photos of representative calcrete samples from the Ziliujing Fm at the Shaping section, Ya'an. *a*, Sample J$_1$*z*-12-01, Bed B12, Ma'anshan Mem; *b*, Sample J$_1$*z*-22-01, Bed B22, Da'anzhai Mem. Pedogenic calcites are light orange and muds are not luminescent. Pedogenic calcites of both samples are evenly luminescent light orange.

Figure 3 Field photographs of climate-sensitive sediments from the Lower Jurassic Ziliujing Fm in GSB. *a*, Reddish purple calcisol with strong leaching structure. Lower Bed H8 of the upper Ma'anshan Mem at Tanba village, Hechuan. *b*, Reddish purple calcisol showing the density and size of calcretes. The horizon and location same as *a*. Arrows point to calcretes. Coin 2.0 cm in diameter. *c,* Reddish purple calcisol with strong leaching structure and rhizoliths. Bed H13 of the top Ma'anshan Mem at

https://doi.org/10.5194/cp-2020-35
Preprint. Discussion started: 13 May 2020

Maliuping, Hechuna. Pen 15 cm long. *d*, Mudcracks. Lower Bed H8 of the upper Ma'anshan Mem at Maliuping, Hechuan. Pen 15 cm long. *e*, Brownish red calcisol with big calcretes (calcareous concretions). Arrows point to big calcretes. Calcisol horizon J_1z-10-01, Bed B10 of Ma'anshan Mem at Shaping village, Ya'an. Hammer 34 cm long. *f*, Chicken-wire structure. Bed H12 of the Da'anzhai Mem at Maliuping village, Hechuan.

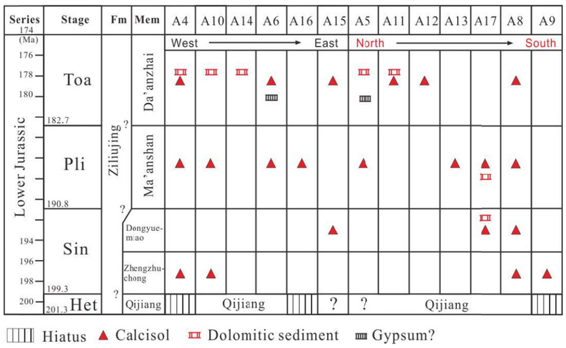

Figure 4 Diagram showing the temporal and spatial variation of climate-sensitive sediments in GSB. Section loactions and data sources refer to Table S2.

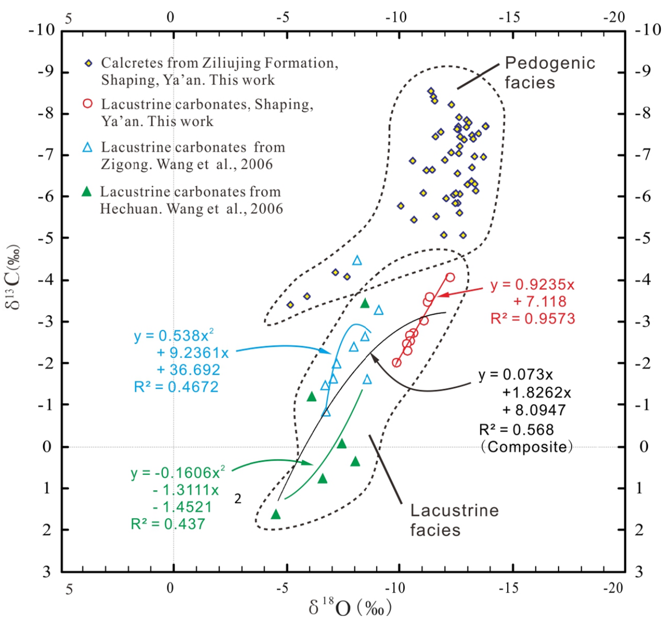

Figure 5 Cross-plot and covariance of carbon and oxygen isotopic values of the Lower Jurassic pedogenic and lacustrine carbonates from GSB. Note, the pronounced covariance (R^2=0.957) between $\delta^{13}C$ and $\delta^{18}O$ from Shaping section, Ya'an, indicating a compositional arid-evaporate and closed pattern lake; the moderate covariance (R^2=0.47 and 0.44) between $\delta^{13}C$ and $\delta^{18}O$ from Zigong and Hechuan, indicating a (semi-) arid and semi-closed pattern lake.

https://doi.org/10.5194/cp-2020-35
Preprint. Discussion started: 13 May 2020

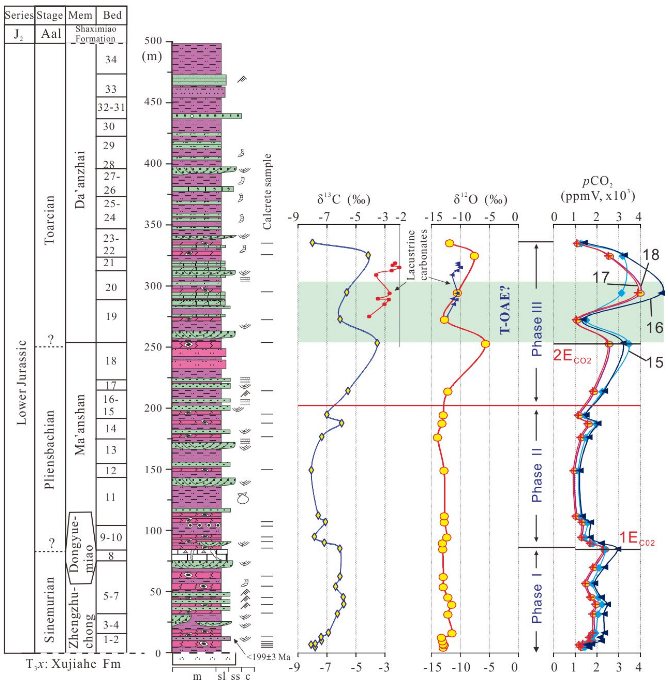

Figure 6 Diagram of the Lower Jurassic strata and litholigcal log at the Shaping section, Ya'an with carbon-oxygen isotope values of pedogenic and lacustrine carbonates and pCO_2 cruve. Three phases and two events can be observed for both stable isotope values of pedogenic carbonates and pCO_2 estimate. T-OAE, Toarcian oceanic anoxic event. $1E_{CO2}$ and $2E_{CO2}$, rapid falling event of pCO_2. Numbers 15 to 18 are the curves of pCO_2 in different parameters, and details refer to supplementary Table S4.

https://doi.org/10.5194/cp-2020-35
Preprint. Discussion started: 13 May 2020

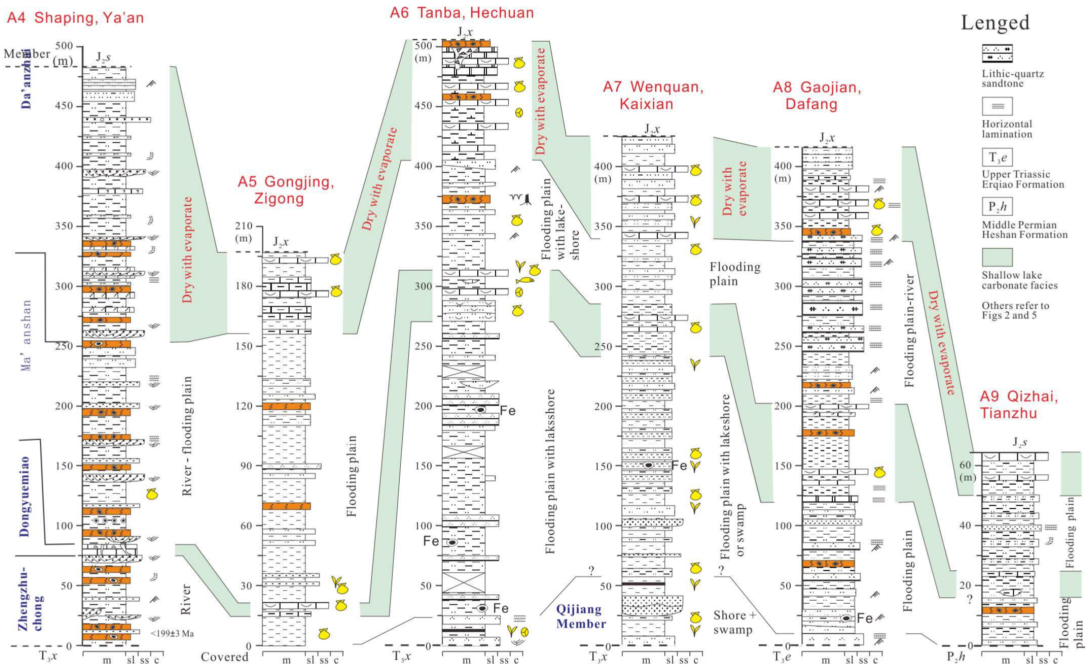

827 **Figure 7 Stratigraphic correlation and depositional environment interpretation of the Lower Jurassic in the GSB. Data of**
828 **sections refer to figure 1 and Table S2. Note, two lacustrine transgressive cycles are marked by correlative pale green areas.**

829

https://doi.org/10.5194/cp-2020-35
Preprint. Discussion started: 13 May 2020

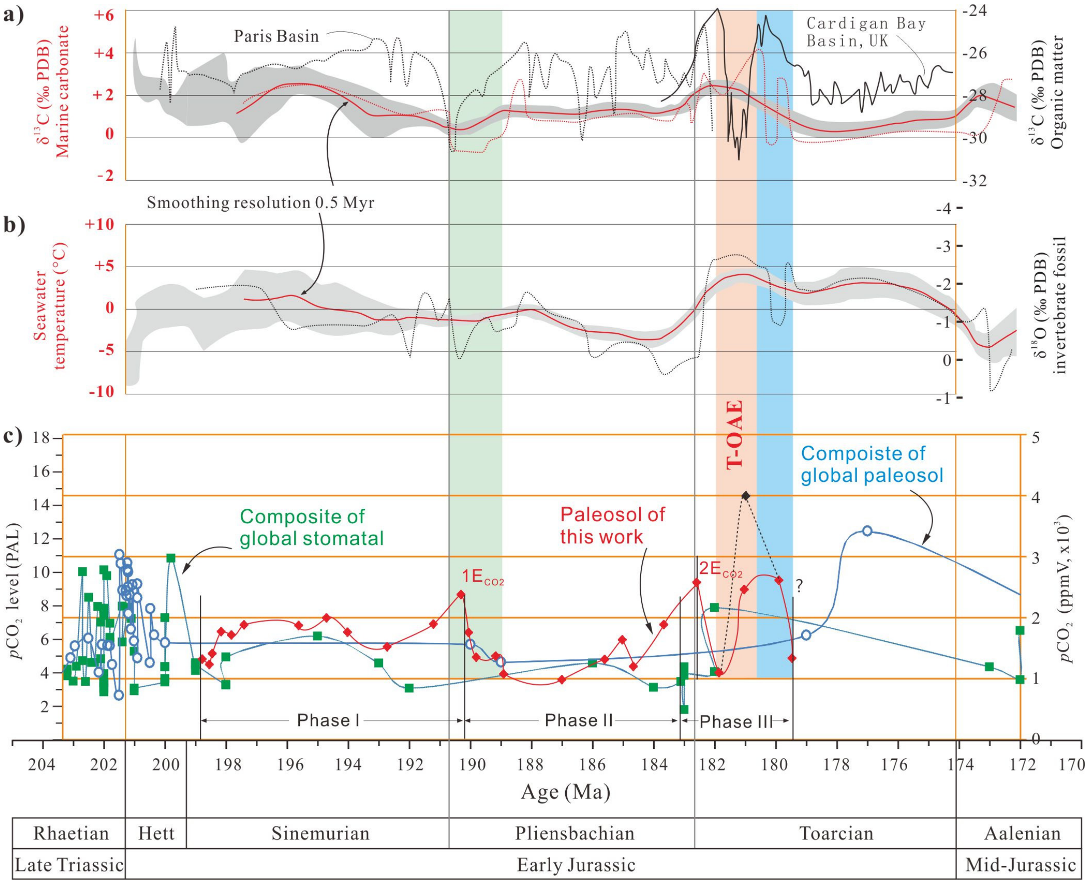

Figure 8 Comparison among the Early Jurassic pCO_2, $\delta^{13}C$ of marine carbonates and organic matters, $\delta^{18}O$ of invertebrate fossils, and seawater temperature. a), $\delta^{13}C$ (red dot line) of marine carbonates composed from Jenkyns and Clayton (1986, 1997), Hesselbo et al. (2000), Dera et al. (2011), Arabas et al., 2017; $\delta^{13}C$ (black dot and solid lines) of organic matters are from Paris Basin, France (Peti et al., 2017) and Cardigan Bay Basin, UK (Xu et al., 2018). b), $\delta^{18}O$ and seawater temperature (black dot line) of marine invertebrate fossils compiled from McArthur et al. (2000), Rosales et al. (2001, 2004), Jenkyns et al. (2002), Bailey et al. (2003), van de Schootbrugge et al. (2005), Gómez et al. (2008), Metodiev and Koleva-Rekalova (2008), Suan et al. (2008), Korte et al. (2009), Dera et al. (2011), Gómez et al. (2016). Smoothed $\delta^{18}O$ and seawater temperature (red curves) in a) and b) are after Dera et al. (2011). c), pCO_2 values, the composite pCO_2 by paleosol and stomatal index collected from the published literatures refer to supplementary Table S5 and S6. Note: 1) pCO_2 = 4027 ppmV (black solid diamond, sample J1z-20-01) if the $\delta^{13}Cr$ = -29.0 ‰ at 181 Ma from Xu et al. (2018) in case of other constant parameters; 2) the early published pCO_2 values from both carbon isotope of pedogenic carbonates and stomatal index of fossil plants (data refer to Table S5 and S6) were awfully rough dated with the average age of a lithostratigraphic formation or group, with which the uncertainty can be upto 10 Myr, leading to the difficulty of precise and accurate pCO_2 correlation in pace, frequency, and event in deep time.

https://doi.org/10.5194/cp-2020-35
Preprint. Discussion started: 13 May 2020

Climate of the Past
Discussions
Open Access

Table

Table 1 Stratigraphic framework of the Lower Jurassic Ziliujing Fm in Sichuan and adjacent area (GSB), Southwest China

Epoch	Age	Formation	W Sichuan (Ya'an)	E Sichuan and Chongqing	S Sichuan and N Guizhou	N Sichuan
Middle Jurassic	Aalenian	Xintiangou Fm	Xintiangou Fm	Xintiangou Fm	Xintiangou Fm	Qianfuyan / Xintiangou Fm
Early Jurassic	Toarcian	Ziliujing Fm	Da'anzhai Mem (Bed 20-34)	Da'anzhai Mem	Da'anzhai Mem	Baitianba Fm
	Pliensbachian		Ma'anshan Mem (Bed 9-18)	Ma'anshan Mem	Ma'anshan Mem	
	Sinemurian		Dongyuemiao Mem (Bed 8)	Dongyuemiao Mem	Dongyuemiao Mem	
			Zhengzhuchong Mem (Bed 1-7)	Zhengzhuchong Mem	Zhengzhuchong Mem	
	Hettangian		**Hiatus**	Qijiang Mem	Qijiang Mem	?
Late Triassic	Rhaetian	Xujiahe Fm	Xujiahe Fm	Xujiahe Fm	Xujiahe Fm	Xujiahe Fm

Notes: Straigraphic classification and correlation were composed from Dong (1984); SBGM (1997), Wang et al. (2010), Wen and Zhao (2010), Xu et al (2017). Re-Os isotope age of the lower Da'anzhai Member is 180.3 ± 3.2 Ma in western Sichuan (Xu et al., 2017). Fm, Formation; Mem, Member.

Supplementary data

Captions of supplemenatary figures

Figure S1 Lithological log of the Lower Jurassic Ziliujing Fm with depositional environment interpretations and sample positions at the Shaping section, Ya'an of Sichuan. Bed number and thickness are partly referred to Wen and Zhao (2010)

Figure S2 Lithological log of the Lower Jurassic Ziliujing Fm at the Tanba-Maliuping section, Hechuan of Chongqing with depositional environment interpretations and sample positions. Bed number and thickness are partly referred to Wang et al (2010).

Figure S3 Field photographs of the Lower Jurassic Ziliujing Fm lithofacies in GSB. *a*, Well roundness and sorting gravels in the alluvial fan conglomerate. Basal and lower Baitianba Fm. Puji, Wangcang. Hammer 30 cm long. *b*, Large trough cross-bedding with scours in the point bar and channel sandstones. Upper Baitianba Fm; Puji, Wangcang. *c*, Calcisol developed within strong leaching overbank mudrocks on channelized sandstones. Middle of Bed B2, the Zhenzhuchong Mem; Shaping section, Ya'an. *d*, Purple red mudrocks intercalated with thin siltstones in flood plain facies. Bed H7 of the Ma'anshan Mem; Tanba section, Hechuan. *e*, Whitish medium-thick micritic dolomites in lacustrine facies. Bed H12 of the Da'anzhai Mem; Maliuping section, Hechuan. Hammer 34 cm long. *f*, Greeinsh gray lacustrine muddy dolomites and dolomitic mudrocks associated with brownish / reddish purple mudrocks. Bed B21 of the Da'anzhai Mem; Shaping section, Ya'an.

Figure S4 Microscopic photos showing lithological microfacies of the Lower Jurassic Ziliujing Fm. *a*, Fine lithic (quartz) sandstone. Lithic-dominant fragments are mudrock. Sample J_1z-02-01b, Zhenzhuchong Mem; Shaping section, Ya'an. Plain-polarised light. *b*, Laminated muddy dolomite and dolomitic mudrocks. Sample J_1z-21S2B, Da'anzhai Mem; Shaping section, Ya'an. Plain-polarised light. *c*, Fine quartz arenite. Sample 18HC-02b3, Bed H2, Qijiang Mem, Tanba section, Hechuan. Cross-polarised light. *d*, Micritic dolomite. Sample 18HC-06b, Bed H12, Da'anzhai Mem. Maliuping section, Hechuan. Plain-polarised light. *e*, Coquina. Shell wall of bivalves were micritized. Mud and recrystalline calcites filled inter-shells and

https://doi.org/10.5194/cp-2020-35
Preprint. Discussion started: 13 May 2020

intra-shells. Sample 18HC-04b, Base of Bed H12, Da'anzhai Mem. Maliuping section, Hechuan. Cross-polarised light. *f*, Relict of coquina. Shell wall of bivalves were parly micritized. Strongly recrystalline calcites replaced the fills and shells. Sample 18HC-05b, Bed H12, Da'anzhai Mem. Maliuping section, Hechuan. Cross-polarised light.

Figure S5 Field photographs of the Lower Jurassic Ziliujing Fm lithofacies in GSB. *a*, Lithofacies and stratigraphic sequence. Beds B8 to B10 of the lower Ma'anshan Mem and Dongyuemiao Mem at Shaping village, Ya'an. *b*, Karstified gravels within the limestone. The horizon and location is same as *a*. Pen 15 cm long. *c*, Layered dolomites with Karstified cave gravels. Bed H12 of the Da'anzhai Mem at Maliuping village, Hechuan. *d*, Karstified cave gravels. The horizon and location is same as *c*. Hammer 34 cm long.

Figure S6 Stratigraphic correlation of the Lower Jurassic Baitianba Fm in northern GSB. Locations and sources refer to Figure 1. Plant fossils and stratal thickness in the Shiguansi section, Wanyuan are cited from SBG (1980b).

Captions of supplemenatary tables

Table S1 Early Jurassic paleosols in Ya'an of Sichuan and Hechuan of Chongqing, Southwest China

Table S2 Carbon-oxygen isotopes of lacustrine carbonates from the Lower Jurassic Ziliujing Fm (Da'anzhai Mem) in the GSB

Table S3 pCO_2 estimate by carbon isotope of pedogenic carbonates from the Lower Jurassic Ziliujing Fm at the Shaping section, Ya'an of Sichuan

Table S4 Occurrence list of the Early Jurassic climate-sensitive sediments in the GSB

Table S5 Global pCO_2 data of the Latest Triassic - Early Jurassic estimated by carbon isotope of pedogenic carbonates

Table S6 Global pCO_2 data of the Latest Triassic - Early Jurassic by stomatal method

Captions of supplemenatary notes

Note S1, Description and interpretation of sedimentary facies and its evolution

Note S2, Notes of parameter usage and selection for the pCO_2 calculation